Origin of primitive ultra-calcic arc melts at crustal conditions — Experimental evidence on the La Sommata basalt, Vulcano, Aeolian Islands

Giovanni Lanzo, Ida Di Carlo, Michel Pichavant, Silvio G. Rotolo, Bruno Scaillet

Highlights

• The experimental phase relations of a natural ultra-calcic arc basalt have been determined

• Results are identical in critical aspects to those obtained previously on a synthetic ultra-calcic arc composition

• Generation of primitive ultra-calcic melt leaves a clinopyroxene-rich residual source, either wehrlite or clinopyroxenite

• Ultra-calcic arc compositions at Vulcano are generated at crustal pressures

• They represent melts produced by the interaction between primary and clinopyroxene-rich wall-rocks

Abstract

To interpret primitive magma compositions in the Aeolian arc and contribute to a better experimental characterization of ultra-calcic arc melts, equilibrium phase relations have been determined experimentally for the La Sommata basalt (Som-1, Vulcano, Aeolian arc). Som-1 ($Na_2O + K_2O$ = 4.46 wt.%, CaO = 12.97 wt.%, MgO = 8.78 wt.%, CaO/Al_2O_3 = 1.03) is a reference primitive *ne*-normative arc basalt with a strong ultra-calcic affinity. The experiments have been performed between 44 and 154 MPa, 1050 and 1150 °C and from NNO + 0.2 to NNO + 1.9. Fluid-present conditions were imposed with H_2O–CO_2 mixtures yielding melt H_2O concentrations from 0.7 to 3.5 wt.%. Phases encountered include clinopyroxene, olivine, plagioclase and Fe-oxide. Clinopyroxene is slightly earlier than olivine in the crystallization sequence. It is the liquidus phase at 150 MPa, being joined by olivine on the liquidus between 44 and 88 MPa. Plagioclase is the third phase to appear in the crystallization sequence and orthopyroxene was not found. Experimental clinopyroxenes ($Fs_{7–16}$) and olivines ($Fo_{78–92}$) partially reproduce the natural phenocryst compositions (respectively $Fs_{5–7}$ and $Fo_{87–91}$). Upon progressive crystallization, experimental liquids shift towards higher SiO_2 (up to ~ 55 wt.%), Al_2O_3 (up to ~ 18 wt.%) and K_2O (up to ~ 5.5 wt.%) and lower CaO, MgO and CaO/Al_2O_3. Experimental glasses and natural whole-rock compositions overlap, indicating that progressive crystallization of Som-1 type melts can generate differentiated compositions such as those encountered at Vulcano. The low pressure cotectic experimental glasses reproduce glass inclusions in La Sommata clinopyroxene but contrast with glass inclusions in olivine which preserve basaltic melts more primitive than Som-1. Phase relations for the La Sommata basalt are identical in all critical aspects to those obtained previously on a synthetic ultra-calcic arc composition. In particular, clinopyroxene + olivine co-saturation occurs at very low pressures (≤ 100 MPa). Ultra-calcic arc compositions do not represent primary mantle melts but result from the interaction between a primary mantle melt and

clinopyroxene-bearing rocks in the arc crust. At Vulcano, primitive ultra-calcic end-member melts were generated between 250 and 350 MPa in the lower magma accumulation zone by reaction between hot primitive melts and wehrlitic or gabbroic lithologies. At Stromboli, golden pumices and glass inclusions with an ultra-calcic affinity were also generated at shallow pressures, between 150 and 250 MPa, suggesting that the interaction model is of general significance in the Aeolian arc.

Keywords : Primitive arc magmas; Ultra-calcic; Experiments; Phase equilibria; Vulcano; Aeolian arc

1. Introduction

Magmas with primitive geochemical characteristics are rare in arc settings. Nevertheless, they occur in virtually every island arc and are of great petrological significance as they constitute a valuable source of information on the nature of source rocks, conditions of partial melting and compositions of primary melts at convergent plate margins. Since different potential source rocks are present in arcs, and conditions of partial melting can be variable, a spectrum of primary magma compositions is expected. Tatsumi and Eggins (1995) defined up to 5 types of primary magmas in subduction zones, shoshonitic, high-, medium- and low-K, and high-Mg andesites (for the latter see Wood and Turner, 2009). Drummond and Defant (1990) proposed additional primary magma types (adakites) generated by melting of the subducted oceanic crust. Arc magmas also include a group of primitive ultra-calcic compositions that are interpreted to be generated from specific but still

poorly constrained mantle source rocks (Schiano et al., 2000; Médard et al., 2004, 2006; Sorbadere et al., 2013).

On a global basis, arc magmas are compositionally evolved because protracted differentiation takes place to produce the typical terms of the arc sequence, from basalt to rhyolite. These differentiation processes tend to mask the geochemical characteristics of the primary magmas. Distinguishing between partial melting (mantle-related) and early differentiation (crust-related) processes is especially difficult for arc magmas (e.g., Takahashi et al., 2013). Yet, for practical petrological and volcanological purposes, it is important to establish the nature of primary magmas, as well as the composition of the most primitive magmas from which the others are derived (e.g., Smith et al., 1997).

In this paper, the above approach is applied to the Aeolian arc, south of the Tyrrhenian Sea. This arc hosts several active reference stratovolcanoes such as Vulcano and Stromboli (Fig. 1). A wide range of compositions, from basalt to rhyolite, erupts along the arc (Peccerillo et al., 2013). Primitive magma compositions are very rare and include calc-alkaline basalts at Alicudi and ultra-calcic compositions at Vulcano and also Stromboli. Glass inclusions from the La Sommata cone on Vulcano are classic examples of primitive ultra-calcic melts in an island arc setting (Schiano et al., 2000). These glass inclusions are also reference samples of natural hydrous basanitic melts (Schiano et al., 2006; Mercier et al., 2010). The La Sommata inclusions occur in olivine and clinopyroxene phenocrysts in a basalt which also displays primitive ultra-calcic characteristics. For our understanding of the magmatic evolution in the Aeolian arc, the petrogenetic significance of such ultra-calcic compositions needs to be evaluated. It is also important to test whether the La Sommata basalt can be a viable parent for the more evolved magmas erupted at Vulcano (De Astis et al., 1997; Gioncada et al., 1998). To achieve these goals, a combined experimental and theoretical approach based on the La Sommata basalt has been undertaken.

Primitive ultra-calcic melt compositions have recently attracted much attention, starting with Schiano et al. (2000). Ultra-calcic compositions from arc settings are silica-poor (SiO_2 as low as 44 wt.%), alkali-rich ($Na_2O + K_2O > 3$ and up to 7 wt.% for the potassic varieties) and *ne*-normative. They have very elevated CaO contents (up to 18 wt.%) and very high CaO/Al_2O_3 ratios (>1.0 and up to 1.6) at moderately high MgO concentrations (8–10 wt.%; compositional data from Schiano et al., 2000; Médard et al., 2004, 2006; Schiano et al., 2006; Mercier et al., 2010; Sonzogni et al., 2010; Rose-Koga et al., 2012; Chen et al., 2013; Fig 2). Liquids with characteristics as above cannot be produced by partial melting of common lherzolitic mantle and their origin is the subject of active research (e.g., Kogiso and Hirschmann, 2001; Green et al., 2004; Schmidt et al., 2004; Médard et al., 2004, 2006; Georgiev et al., 2009; Marchev et al., 2009; Sorbadere et al., 2013). At present, the origin of ultra-calcic arc compositions is only constrained from experimental data obtained on a volatile-free synthetic mixture (Médard et al., 2004). Experimental data on natural ultra-calcic arc rocks and in presence of volatiles are lacking. Yet, the primitive basalt from La Sommata has a bulk composition close to the synthetic mixture investigated by Médard et al. (2004); in particular, CaO/Al_2O_3 and wt.% MgO are almost identical (Fig. 2). Therefore, this composition offers the opportunity to document the phase relations of a representative ultra-calcic arc basalt. The experimental results presented in this paper contribute to a better experimental characterization of ultra-calcic arc melts in general and enable their origin to be further discussed.

2. Regional, petrological and volcanological background and starting material

2.1. Primitive compositions in the Aeolian arc

The Aeolian archipelago (Fig. 1) represents a Pleistocene volcanic arc whose origin is related to the westward subduction of the Ionian plate below the Calabrian-Peloritan thrust belt, in the context of the south-eastern propagation of the Tyrrhenian basin, following the rollback of the Ionian slab (e.g., Ventura, 2013). The Aeolian arc consists of seven subaerial volcanic edifices (Alicudi, Filicudi, Salina, Lipari, Vulcano, Panarea and Stromboli) and several volcanic seamounts surrounding the Marsili basin (Fig. 1). The volcanic activity of the Aeolian Islands

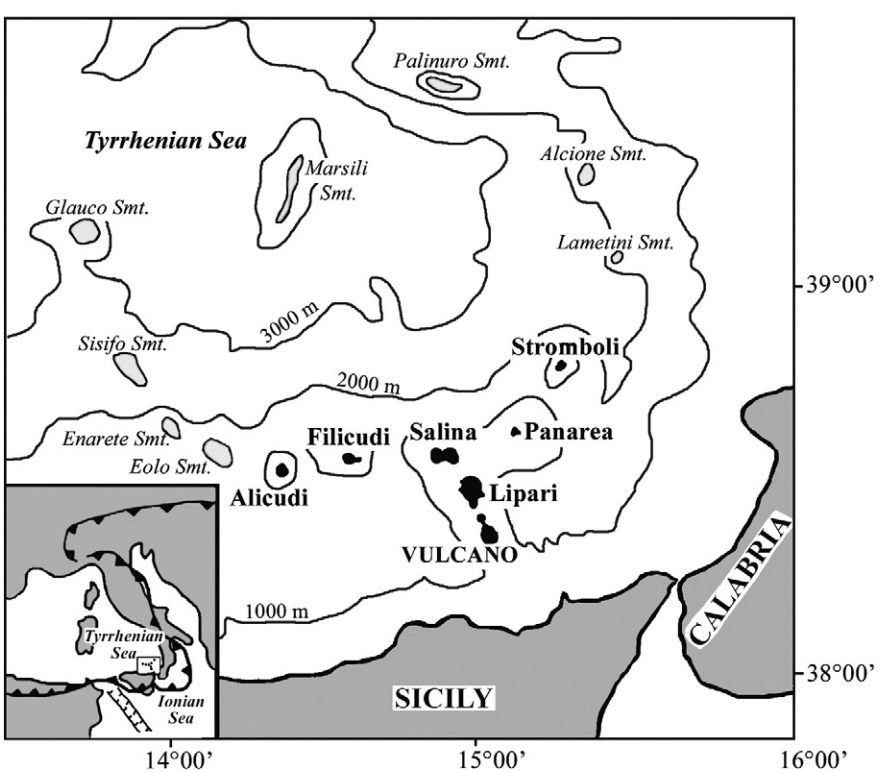


Fig. 1. Sketch map of the Tyrrhenian Sea basin showing the location of the Aeolian Arc and of the seven subaerial volcanic edifices and seamounts discussed in text. The inset shows the general geodynamic context including the Africa-Eurasia boundary, the Sicily channel extension system and the location of the Aeolian domain (square).

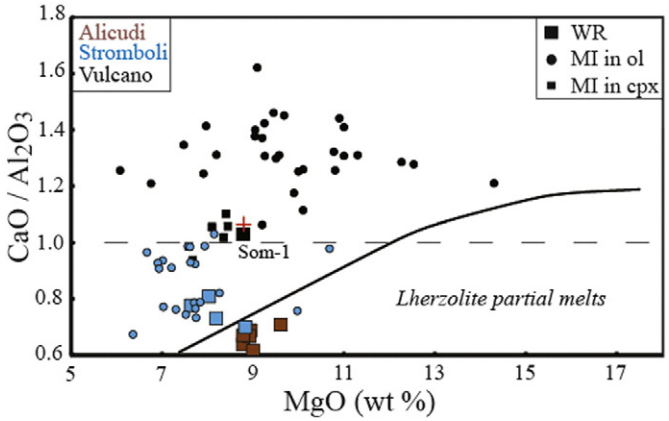


Fig. 2. CaO/Al_2O_3 vs. MgO plot showing primitive compositions in the Aeolian arc. Compositions from Alicudi, Stromboli and Vulcano are distinguished by different colours, respectively brown, blue and black. Whole-rock (WR) compositions are plotted as large filled squares, melt inclusions (MI) in olivine as filled circles and MI in clinopyroxene as small filled squares. The red cross is the ultra-calcic arc synthetic mixture CaNe (Médard et al., 2004). Source of data, La Sommata: WR (Som-1) from Table 1, MI (data corrected for post-entrapment crystallization and normalized to 100%) from Métrich and Clocchiatti (1996); Gioncada et al. (1998); Schiano et al. (2000, 2006); Mercier et al. (2010); Sonzogni et al. (2010); Rose-Koga et al. (2012) and Chen et al. (2013). Note that Som-1 and CaNe are almost coincident. Source of data, Stromboli: WR from Pichavant et al. (2011), MI data from Bertagnini et al. (2003). Source of data, Alicudi: WR from Peccerillo (2005). The curve limiting the compositional domain of lherzolite partial melts is taken from Médard et al. (2004). The horizontal dashed line separates the ultra-calcic ($CaO/Al_2O_3 > 1$) and non-ultra-calcic ($CaO/Al_2O_3 < 1$) fields.

started about 1.3 My ago (Ventura, 2013) and is still active on three of the seven major islands, Lipari (last eruption in 1230 AD; Arrighi et al., 2006), Stromboli (persistently active), and Vulcano (last eruption in 1888–1890). Rock compositions range from basalt to rhyolite and belong dominantly to the calc-alkaline, high-K calc-alkaline and shoshonitic series, more rarely to the potassic series (see for instance Peccerillo et al., 2013). In detail, the arc is segmented in three main sectors and magma compositions vary both at the local and regional scales, and also with time at a given volcano. There is a general agreement that the erupted mafic compositions originate from primary magmas produced by partial melting of an heterogeneous mantle source, and follow a complex polybaric evolution in the arc crust (Peccerillo et al., 2013 and references therein). Primitive magma compositions rarely occur. They include products mainly from Alicudi and Vulcano islands (Fig. 1). The calc-alkaline basalts from Alicudi have the most primitive whole-rock major and trace element characteristics of the entire Aeolian arc, with Mg# up to 73, Ni up to 150 ppm and Cr up to 800 ppm (Peccerillo et al., 2004). These basalts contain 50.4–51.7 wt.% SiO_2, 0.93–1.38 wt.% K_2O and 8.78–9.61 wt.% MgO, have CaO/Al_2O_3 ranging from 0.64 to 0.71, are *hy*-normative and plot in the field of primary melts from lherzolitic mantle (Fig. 2). Rocks with similar characteristics (48.6–50.5 wt.% SiO_2, 0.84–1.26 wt.% K_2O, 8.43–8.48 wt.% MgO, 70–297 ppm Cr, 68–109 ppm Ni, $CaO/Al_2O_3 < 0.5$) have been dredged in the lowermost slope north of Alicudi and Filicudi (Beccaluva et al., 1985).

At Vulcano, the La Sommata basalt is the most primitive eruptive product (De Astis et al., 1997; Gioncada et al., 1998). The scoria sample used in this study (Som-1) is a shoshonitic basalt with 49.55 wt.% SiO_2, 2.28 wt.% K_2O and 8.78 wt.% MgO when normalized to 100% (Table 1). It is *ne*-normative (5% *ne*), has an elevated CaO/Al_2O_3 (1.03) and plots in the ultra-calcic field (Schiano et al., 2000; Fig 2), as the La Sommata glass inclusions (MI). Numerous studies have been performed on the La Sommata MI, mostly on inclusions in olivine phenocrysts (Métrich and Clocchiatti, 1996; Gioncada et al., 1998; Schiano et al., 2000, 2006; Mercier et al., 2010; Rose-Koga et al., 2012; Chen et al., 2013), but also in clinopyroxene (Sonzogni et al., 2010). The La Sommata MI (Table 1) have 46.5–50.5 wt.% SiO_2, 1.34–2.83 wt.% K_2O and 6.08–14.30 wt.% MgO and are characterized by high CaO/Al_2O_3 ratios between 1.0 and 1.6, typical of the ultra-calcic signature (Schiano et al., 2000, Fig. 2). These MI are strongly *ne*-normative (*ne* up to 10%) and hydrous. FTIR analyses have yielded a range of dissolved H_2O concentrations between 1.8 and 3.8 wt.% (Gioncada et al., 1998). More recently, Mercier et al. (2010) analyzed 3.8–4.5 wt.% H_2O in olivine-hosted inclusions by Raman microspectroscopy. The latest measurements have yielded 0.6–4.9 wt.% H_2O by SIMS (Rose-Koga et al., 2012) and 1.0–5.3 wt.% H_2O with a new Raman-FTIR calibration (Chen et al., 2013).

Primitive compositions also occur at Stromboli. Basaltic rocks there cluster near 6–7 wt.% MgO for 10–11 wt.% CaO, and a few samples have >7.5 wt.% MgO (see Pichavant et al., 2011 for a recent compilation). The high-MgO group includes, in the recent period of activity, one golden pumice erupted during a paroxysm, and, in the older periods, one sample from the Younger Series and two dyke samples (see Pichavant et al., 2011 and references therein, Fig. 2). The golden pumice (PST-9) has 7.71 wt.% MgO, 239 ppm Cr and 67 ppm Ni (Pichavant et al., 2009, 2011). It displays a clear calcic signature with 12.48 wt.% CaO and $CaO/Al_2O_3 = 0.80$ (Pichavant et al., 2011). In comparison, the other primitive Stromboli samples have lower CaO and CaO/Al_2O_3 (Fig. 2). Fo-rich olivines in golden pumices host glass inclusions with ~49 wt.% SiO_2, ~2 wt.% K_2O and MgO up to >8 wt.% (corrected for post-entrapment crystallization). They have CaO/Al_2O_3 ranging from 0.67 up to 1.03 (Fig. 2) and are *ne*-normative (~5% *ne*, Bertagnini et al., 2003; Métrich et al., 2010; Pichavant et al., 2011), and display a strong ultra-calcic affinity (Schiano et al., 2000; Pichavant et al., 2009).

We conclude to the occurrence of two main groups of primitive magma compositions in the Aeolian arc. Primitive calc-alkaline magmas are found on Alicudi (Peccerillo et al., 2004), possibly also among rocks dredged on seamounts (Beccaluva et al., 1985). Both primitive ultra-calcic rocks and MI are well represented on Vulcano and they also occur at Stromboli, although with a less marked ultra-calcic imprint. The presence of ultra-calcic characteristics both at Vulcano and Stromboli suggests that this specific geochemical signature is widespread in the Aeolian arc. It is worth mentioning that high-Ca inclusions in high Fo olivines are also found in south Italy but outside the Aeolian arc (e.g., Mt. Maletto, Kamenetsky and Clocchiatti, 1996).

2.2. The island of Vulcano: volcanological background

Vulcano is the southernmost island of the Aeolian archipelago (Fig. 1). Its geological evolution encompasses the last 130 ka (to the last 1888–1890 eruption) in seven main eruptive epochs marked by major unconformities, caldera collapses and quiescence periods (see De Astis et al., 2006, 2013, for details). Erupted magmas at Vulcano cover the widest compositional range of the whole Aeolian archipelago, from silica-undersaturated potassic rocks to rhyolites, and spread the high potassium calc-alkaline (HKCA) and shoshonite (SHO) suites (Keller, 1974; De Astis et al., 1997, 2000), with a general increase of potassium content with time. The older products (120–30 ka) are characterized by a silica content <56 wt.%, whilst the younger products (<30 ka) include more silicic and potassic rocks (De Astis et al., 2013). The pre-30 ka activity erupted the most primitive products.

In detail, the most mafic compositions (MgO = 6.1–8.8 wt.%, De Astis et al., 1997) were mainly erupted between 80 and 30 ka and are related to the Il Piano Synthem, within the Piano Caldera (De Astis et al., 2006). These products are represented by the Passo del Piano lava (Mg# = 0.57, $CaO/Al_2O_3 = 0.65$, De Astis et al., 1997) and the Monte Rosso trachybasalt (Mg# = 0.52, $CaO/Al_2O_3 = 0.64–0.73$; De Astis et al., 1997; Gioncada et al., 1998), all with lower Mg#, wt.% MgO and CaO/Al_2O_3 than the La Sommata basalt (ca. 41 ka B.P., C.A. Tranne, personal communication, 2014). Previous analyses of this basalt (Mg# = 0.57–0.59, MgO = 8.07–8.64 wt.%, $CaO/Al_2O_3 = 0.90–1.0$, De Astis et al., 1997; Gioncada et al., 1998) are consistent with our own results (Table 1). They confirm the primitive characteristics of the La Sommata basalt and stress its specific ultra-calcic composition.

Table 1
Compositional and modal data for the La Sommata basalt sample used in the experiments.

	SiO_2	TiO_2	Al_2O_3	FeO_t	MnO	MgO	CaO	Na_2O	K_2O	P_2O_5	Cr_2O_5	Total	CaO/Al_2O_3		Mg#	Phenocryst abundance (vol.%)
Som-1																
Glass (n = 179)	49.55 (0.3)	0.74 (0.0)	12.66 (0.2)	10.23 (0.3)	0.21 (0.1)	8.78 (0.1)	12.97 (0.2)	2.18 (0.1)	2.28 (0.1)	0.40 (0.0)	–	98.02	1.03		60	
Groundmass																
(n = 20)	53.12 (1.0)	0.64 (0.1)	19.95 (1.4)	7.33 (1.0)	0.19 (0.1)	1.18 (0.5)	4.54 (1.7)	4.97 (0.4)	6.73 (1.0)	0.77 (0.2)	–	97.74	0.23		20	
Clinopyroxene													**En**	**Fs**		7
Phenoxtal	54.69 (0.7)	0.2 (0.1)	1.88 (0.1)	3.18 (0.5)	0.13 (0.0)	16.73 (0.8)	22.87 (1.1)	0.56 (0.0)	0.0 (0.0)	0.0 (0.0)	–	98.45	48	5	90	
MicPheno	53.47 (1.6)	0.43 (0.1)	3.15 (1.3)	4.52 (1.2)	0.14 (0.0)	16.04 (1.1)	21.88 (0.4)	0.52 (0.1)	0.0 (0.0)	0.04 (0.0)	–	99.07	47	7	86	
MicLit	50.72 (2.0)	0.70 (0.3)	5.30 (2.2)	6.88 (1.2)	0.12 (0.0)	13.94 (1.8)	21.78 (0.7)	0.62 (0.2)	0.08 (0.1)	0.0 (0.0)	–	98.06	42	12	78	
Olivine													**Fo**			3
Phenoxtal	41.49 (0.2)	0.03 (0.0)	0.05 (0.0)	8.93 (0.3)	0.18 (0.1)	48.37 (0.2)	0.39 (0.0)	0.71 (0.1)	0.04 (0.0)	0.0 (0.0)	–	99.42	91			
MicPheno	41.86 (0.8)	0.04 (0.0)	0.05 (0.0)	9.4 (2.3)	0.24 (0.1)	47.84 (1.8)	0.34 (0.0)	0.74 (0.1)	0.03 (0.0)	0.06 (0.1)	–	99.35	90			
MicLit	40.30 (1.0)	0.03 (0.1)	0.05 (0.1)	15.65 (6.1)	0.41 (0.2)	42.33 (5.4)	0.48 (0.2)	0.85 (0.2)	0.0 (0.0)	0.03 (0.1)	–	97.58	83			
Plagioclase													**An**	**Ab**		0.3
Phenoxtal	51.74	0.10	30.71	1.09	0.0	0.02	11.64	3.96	0.82	0.0	–	98.91	59	36		
MicPheno	51.36 (0.7)	0.1 (0.1)	31.84 (0.2)	0.92 (0.1)	0.04 (0.0)	0.01 (0.0)	11.85 (0.6)	3.79 (0.1)	0.58 (0.0)	0.0 (0.0)	–	98.67	61	35		
MicLit	51.26 (1.0)	0.15 (0.1)	31.02 (1.3)	1.26 (0.6)	0.07 (0.1)	0.11 (0.2)	11.62 (0.8)	3.77 (0.4)	0.96 (0.6)	0.01 (0.0)	–	98.40	59	35		
Spinel													**Cr#**	**Usp**		<.1
MicPheno	0.11 (0.1)	0.56 (0.1)	8.87 (0.4)	26.03 (0.8)	0.24 (0.2)	11.52 (0.3)	0.07 (0.1)	0.66 (0.2)	0.0 (0.0)	0.01 (0.0)	52.00 (0.4)	92.35	80	–		
MicLit	1.32 (1.4)	6.96 (1.8)	7.41 (1.5)	78.65 (2.2)	0.47 (0.2)	3.30 (0.6)	0.45 (0.2)	1.07 (0.2)	0.17 (0.3)	0.06 (0.1)	0.59 (0.4)	86.46	–	23		
Glass inclusions																
in olivine not recalculated	45.28	0.54	11.06	7.85	0.18	8.53	14.45	2.03	1.94	0.28	–	92.14	1.31		$^*Fo_{90}$	
in olivine recalculated	48.8	0.7	12	9.6	0.2	9.9	14.1	2.2	2.1	0.33	–	–	1.18		$^*Fo_{88}$	
in clinopyroxene	46.89	0.99	11.8	11.69	0.25	7.71	12.45	1.94	1.28	0.24	–	95.24	1.05		$^*Fs_6$	
Prim-1																
calculated	47.73	0.74	11.25	10.76	0.22	10.25	14.60	2.13	1.90	0.42	–	100.00	1.30			

Som-1 starting glass (after melting of whole rock) average and standard deviations (in brackets) were calculated on *179* analyses. **En** = 100 * Mg/(Mg + Fe + Ca), **Fs** = 100 * Fe/(Mg + Fe + Ca), **An** = 100 * Ca/(Ca + Na + K), **Ab** = 100 * Na/(Ca + Na + K). Mg# = Mg/(Mg + Fe); **Cr#** = Cr/(Cr + Al). All Fe as FeO_t. All analyses are reported on a 100% basis, the original totals being given. Modal analyses (void-free) by point counting on 3600 points. Representative analyses of olivine-hosted glass inclusions: not recalculated for post-entrapment crystallization from Gioncada et al. (1998), recalculated for post-entrapment crystallization from Rose-Koga et al. (2012); glass inclusion in clinopyroxene (not recalculated) from Sonzogni et al. (2010). Asterisk labels the composition of the host crystals. Prim-1 is the theoretical composition of a primitive end-member magma; see text for details.

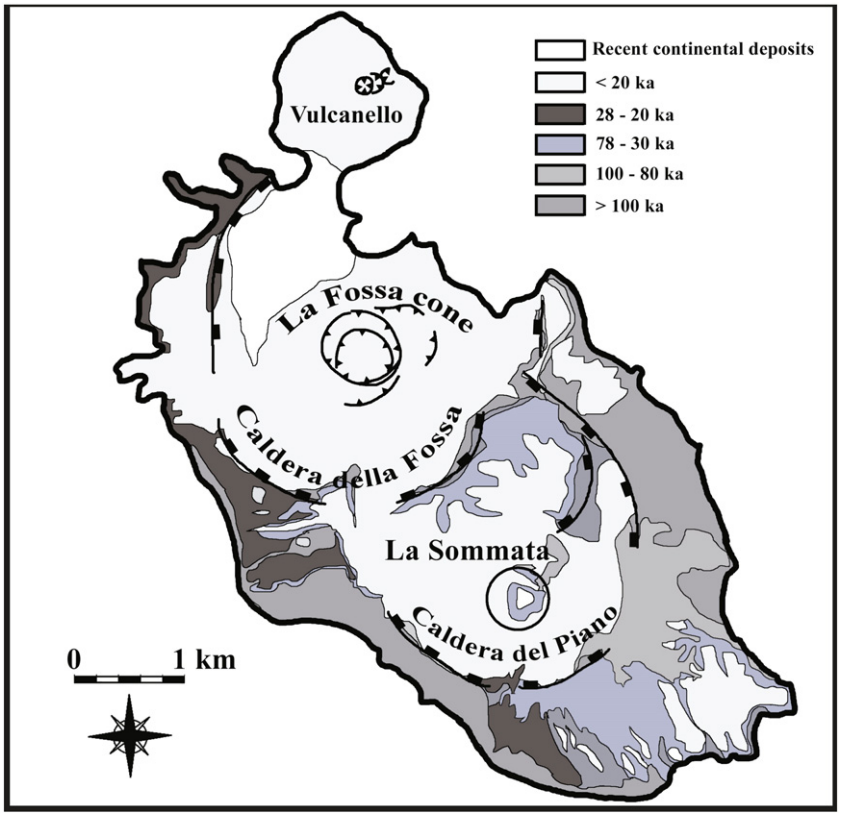


Fig. 3. Geological sketch map of Vulcano island, showing the distribution of the volcanic units erupted during the five different periods of activity (modified from De Astis et al., 2006). The La Sommata cone is located in the southern portion of the island, within the Caldera del Piano.

La Sommata is a scoria cone built close to the southern rim of the Caldera del Piano (Fig. 3). Its products consist of vesiculated scoriaceous lapilli, dense scoria bombs and subordinate centimetric lava lithic blocks that originated from a fluctuating strombolian-type activity. Primitive major and trace element characteristics and low $^{87}Sr/^{86}Sr = 0.7042$ (De Astis et al., 1997) have led Gioncada et al. (1998) to propose the La Sommata basalt as representative of parental magmas that fed the pre-Lentia caldera activity (older than 15 ka B.P.). However, the magmatic evolution at Vulcano is more complex than differentiation of a single parental magma and the importance of open-system and magma mixing processes has been emphasized in several studies (De Astis et al., 1997, 2013; Del Moro et al., 1998; Gioncada et al., 1998; Clocchiatti et al., 1994; Piochi et al., 2009).

2.3. The La Sommata basalt: petrography and mineralogy

We selected for our purposes only vesiculated scoriaceous lapilli, distinctly less porphyritic than scoriaceous bombs. Point counting showed the presence of ca. 10 vol.% phenocrysts on a vesicle-free basis (Table 1). The hybrid nature of the phenocryst population has been recognized previously and Gioncada et al. (1998) estimated that the La Sommata basalt represents a product of mixing between a primitive and a more evolved shoshonitic magma in a 80:20 proportion. Accordingly, the phenocryst assemblage is divided into two groups:

(1) a *basaltic assemblage*, which comprises clinopyroxene (Cpx), olivine (Ol) and Cr-spinel (Sp). Diopsidic clinopyroxene ($En_{48-49}Fs_{5-7}$, X_{Mg} = molar MgO/(MgO + FeO_{tot}) = 0.87–0.92) is the most abundant phase (Table 1). Olivine is Fo-rich (Fo_{87-91}). Spinel is a chromite with Cr_2O_3 up to 52 wt.% and Cr# (at. 100 * Cr/(Cr + Al)) up to 82. Both clinopyroxene and spinel can be found included in olivine. Petrographic observations suggest cotectic crystallization of olivine and clinopyroxene phenocrysts (Fig. 4).

(2) a *shoshonitic assemblage*, which is characterized by phenocrysts and microphenocrysts of salitic clinopyroxene ($En_{36-44}Fs_{10-16}$), olivine (Fo_{68-84}) and rare plagioclase (An_{55-66}).

The groundmass (bulk composition $SiO_2 = 53.1$ wt.%, $K_2O/Na_2O = 1.35$, Table 1) is extensively crystallized (Fig. 4). Plagioclase is very abundant and Ti-magnetite is also present.

Clinopyroxene-liquid and olivine-liquid equilibria were checked by calculating Fe–Mg mineral–liquid partition coefficients with the bulk Som-1 rock taken as the liquid composition (Som-1 glass, Table 1). A range of fO_2 between NNO + 0.5 to NNO + 2 was considered to compute the liquid FeO concentration (Kress and Carmichael, 1991), yet the conclusions of the calculations are almost independent of the choice of fO_2. The most Fs-poor Cpx and Fo-rich Ol phenocrysts of the basaltic assemblage are out of equilibrium with Som-1. Only evolved clinopyroxenes ($Fs \geq 7$, $X_{Mg} \leq 0.87$) and olivines ($Fo < 88$) approach equilibrium with the bulk rock. So, the most primitive phenocrysts (Fs_5, Fo_{91}) are in fact xenocrysts, interpreted to have crystallized from a liquid more primitive than Som-1. This crystallization stage presumably occurred prior to mixing with the shoshonitic magma (Gioncada et al., 1998). Therefore, Som-1 does not correspond exactly to an end-member primitive liquid. However, the La Sommata basalt is almost identical to typical ultra-calcic arc compositions such as the synthetic mixture CaNe experimentally investigated by Médard et al. (2004), being also close to compositions of MI in La Sommata clinopyroxene (Fig 2). Therefore, Som-1 can be viewed as a reasonable natural approximation of an ultra-calcic arc melt.

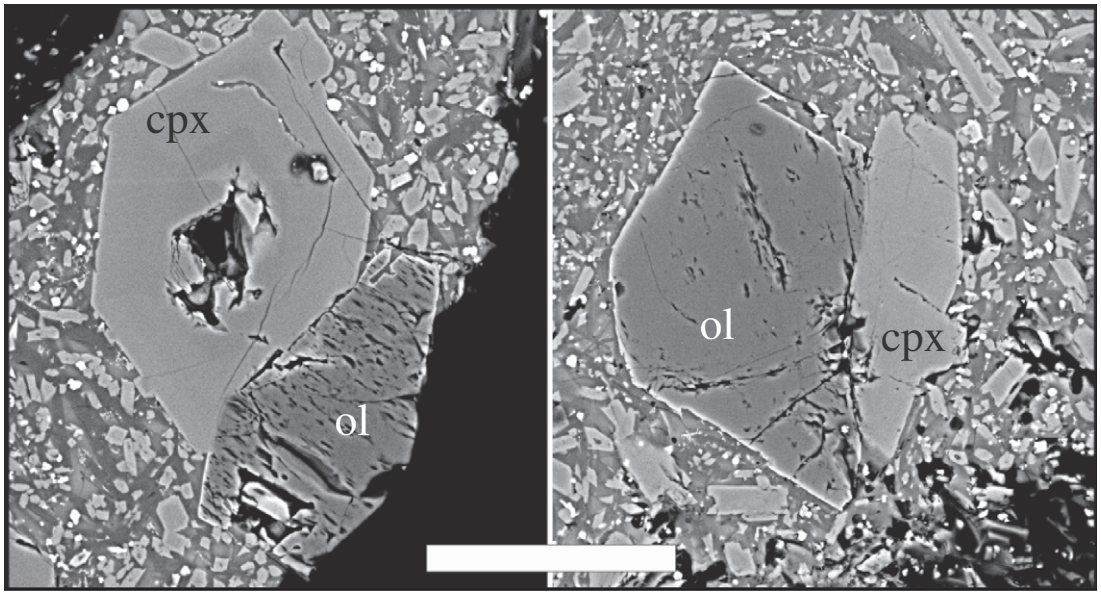


Fig. 4. Back-scattered electron microphotographs of the La Sommata basalt sample showing olivine (ol) and clinopyroxene (cpx) phenocrysts of the basaltic assemblage and their textural relations consistent with cotectic crystallization. Notice the extensively crystallized groundmass.

3. Experimental and analytical techniques

3.1. Experimental strategy

The choice of experimental T-P-H_2O conditions was guided by previous experimental studies on similar compositions (Médard et al., 2004; Di Carlo et al., 2006) and also by the range of water contents of the glass inclusions (Gioncada et al., 1998; Mercier et al., 2010; Chen et al., 2013). Accordingly, experiments were carried out at pressures between 150 and 50 MPa and temperatures between 1150 and 1050 °C. An isobaric section at 150 MPa, corresponding to the highest water concentrations measured in the glass inclusions (Gioncada et al., 1998; Mercier et al., 2010; Chen et al., 2013), was investigated in detail. An isothermal section at 1150 °C was also studied, the latter being a reasonable crystallization temperature for phenocrysts in La Sommata basalt on the basis of homogenization temperatures of glass inclusions (Gioncada et al., 1998) and of calculations using the MELTS software (Chen et al., 2013).

Experimental redox conditions above the NNO buffer were imposed to match the oxidizing fO_2 of the La Sommata rock. Olivine-spinel oxybarometry (Ballhaus et al., 1991) yields a $\Delta NNO = +1.8$ using mineral compositions from Table 1. In comparison, a $\Delta NNO = +0.72$ was determined by Métrich and Clocchiatti (1996) from S^{6+}/S_{tot} ratios in La Sommata melt inclusions, so less oxidizing but in agreement with the fO_2 range implied by olivine-spinel oxybarometry (>NNO).

3.2. Preparation of the starting material

A batch of 20 g of Som-1 scoriae was finely crushed (down to 30–50 μm size) then melted twice in a platinum crucible at 1400 °C for 3 h in air, with grinding in between. A few glass chips were taken and ground to produce the starting powdered dry glass material. Depending on experimental temperatures, capsules were made of either Au, $Au_{90}Pd_{10}$ or $Au_{80}Pd_{20}$ tubing (15 mm length, 2.5 mm internal diameter, 0.2 mm wall thickness). All experiments were performed under fluid-present conditions. The initial composition of the fluid phase ranged from pure H_2O to pure CO_2. CO_2 was added only to reduce experimental aH_2O and so to control the melt H_2O content since glass inclusions in La Sommata basalt contain no detectable CO_2 (Gioncada et al., 1998). Distilled water was first introduced with a microsyringe, then CO_2 (as silver oxalate), and finally 30 mg of the powdered dry glass (Table 1). The capsules were then arc welded in a liquid nitrogen bath in order to prevent water loss. After welding, the capsules were weighed and then left in an oven at 110 °C for 2 h to homogenize the water distribution in the charge. For each experiment at given P-T conditions, 3 to 5 capsules were run together, each with different starting XH_2O [= molar $H_2O/(H_2O + CO_2)$] ranging from 1 to 0.

3.3. Experimental equipment

All experiments were carried out in an Internally Heated Pressure Vessel (IHPV) working vertically, pressurized with H_2–Ar gas sequentially loaded at room temperature (Scaillet et al., 1992, 1995) and equipped with a fast quench device modified after Roux and Lefevre (1992). The experimental charges were loaded into an alumina sample holder hung in the hot zone of a furnace made of a double parallel Mo winding. Pressure was recorded by a transducer calibrated against a Heise Bourdon tube gauge with an uncertainty of ±20 bars. Two S-type thermocouples allowed a continuous control of the temperature in the top and the bottom of the hot-spot (i.e. for a length of 5 cm). The temperature gradient in the hot-spot zone was always <5 °C. At the end of the experiment, the Pt wire hanging the sample holder was fused electrically allowing the experimental charges to fall in the cold part of the vessel in a few seconds (Di Carlo et al., 2006).

3.4. Control and monitoring of oxygen fugacity

The use of a H_2-Ar gas mixture of fixed composition imposes a given partial pressure of hydrogen (fH_2) in each experiment, which in turn allows the fO_2 to be determined for each charge (e.g., Scaillet et al., 1992; Di Carlo et al., 2006). For a given experiment (hence fixed fH_2), the fO_2 of a given charge is dependent on the melt H_2O concentration (H_2O_{melt}). The fO_2 for each capsule was calculated from the water dissociation equilibrium ($K_w = fH_2O/(fH_2 * fO_2^{0.5})$ with K_w taken from Robie et al. (1979) and fH_2O calculated from H_2O_{melt} using the model of Burnham (1979). The experimental fH_2 was determined by using an empirical calibration between the H_2 pressure initially loaded in the vessel and the fH_2. The latter was obtained from other experimental runs performed at the same P-T conditions using the same vessel and procedure than in the present study, and where experimental fH_2 were determined with Ni-Pd sensors (e.g., Di Carlo et al., 2006).

Table 2
Experimental conditions.

Charge	H_2O_{melt} (wt.%)	aH_2O	log fO_2	ΔNNO	Phase assemblage	$\sum R^2$	ΔFeO (%)	$K_d^{Fe-Mg}{}_{cpxliq}$	$K_d^{Fe-Mg}{}_{ol-liq}$	$K_d^{Ca-Na}{}_{pl-liq}$
Som-1										
Run 2, 1150 °C, 153.9 MPa, 23 h, fH_2 = 0.163 MPa, $Au_{80}Pd_{20}$.										
(2-1)	3.52 (*3.45*)	0.994	−6.46	1.83	gl(100) + ox(tr)	0.2	−1.58			
(2-2)	3.15 (*3.13*)	0.873	−6.58	1.72	gl(100) + ox(tr)	0.1	−5.62			
(2-3)	2.69	0.662	−6.82	1.48	gl(90) + cpx(10) + ox(tr)	0.1	−2.29	0.262		
(2-4)	1.74	0.305	−7.49	0.80	gl(79) + cpx(20) + ol(1) + ox(?)	0.0	−11.46	0.228	0.235	
(2-5)	1.20	0.158	−8.06	0.23	gl(74) + cpx(24) + ol(2) + ox(tr)	0.0	−4.81	0.288	0.277	
Run 5, 1120 °C, 140.84 MPa, 20 h, fH_2 = 0.129 MPa, $Au_{80}Pd_{20}$.										
(5-1)*qc*	3.45	0.923	−6.79	1.87	gl(100) + ox(tr)					
(5-2)*qc*	2.84	0.629	−7.12	1.54	gl(79) + cpx(17) + ol(2) + ox(2)	0.3	−0.73	0.192	0.170	
(5-3)	2.55	0.484	−7.35	1.31	gl(75) + cpx(21) + ol(2) + ox(2)	0.1	−0.81	0.287	0.216	
(5-4)	1.45	0.202	−8.11	0.55	gl(64) + cpx(33) + ol(0.4) + ox(3)	0.3	−1.89	0.252	0.245	
(5-5)	1.21	0.145	−8.39	0.27	gl(63) + cpx(34) + ol(3) + pl(tr) + ox(tr)	0.1	−7.11	0.216	0.209	1.49
Run 8, 1080 °C, 146.3 MPa, 21.5 h, fH_2 = 0.132 MPa, $Au_{90}Pd_{10}$.										
(8-1)	3.34	0.709	−7.60	1.58	gl(65) + cpx(31) + ol(tr) + ox(3)	0.8	−0.28	0.291		
(8-2)	2.01	0.311	−8.31	0.86	gl(51) + cpx(45) + ol(0.4) + ox(3.6)	0.9	−3.31	0.314	0.265	
(8-3)	1.41	0.186	−8.76	0.41	gl(46) + cpx(50) + ol(1) + pl(tr) + ox(3)	0.0	−1.08	0.303	0.285	
Run 7, 1050 °C, 159.43 MPa, 25.7 h, fH_2 = 0.0.131 MPa, Au.										
(7-5)	3.37	0.637	−8.08	1.50	gl(61) + cpx(33) + ol(2) + ox(4)	1.0	−3.19	0.397	0.247	
(7-6)	2.20	0.327	−8.66	0.92	gl(50) + cpx(45) + ol(0.4) + pl(tr) + ox(4.6)	0.1	−0.72	0.315	0.299	
Run 3, 1150 °C, 87.5 MPa, 21 h, fH_2 = 0.120 MPa, $Au_{80}Pd_{20}$.										
(3-1)*qc*	2.43	0.870	−6.86	1.44	gl(100)					
(3-2)*qc*	2.17	0.720	−7.02	1.28	gl(91) + cpx(9) + ol(tr) + ox(tr)	0.1	−0.72	0.244	0.176	
(3-3)*qc*	1.93	0.590	−7.20	1.11	gl(87) + cpx(13) + ol(0.2) + ox(tr)	0.4	−5.95	0.212	0.175	
(3-4)	1.55	0.370	−7.60	0.70	gl(79) + cpx(19) + ol(2) + ox(tr)	0.2	−3.10	0.295	0.254	
(3-5)	1.25	0.240	−7.98	0.33	gl(74) + cpx(23) + ol(3) + ox(?)	0.1	−7.80	0.302	0.284	
Run 6, 1150 °C, 44.07 MPa, 20.1 h, fH_2 = 0.122 MPa, $Au_{80}Pd_{20}$.										
(6-1)	1.95 (*2.17*)	0.990	−7.29	1.02	gl(100) + ox(tr)	0.2	−4.84			
(6-2)	1.89 (*1.94*)	0.940	−7.34	0.97	gl(100) + ox(tr)	0.4	−3.32			
(6-3)	1.62	0.720	−7.57	0.74	gl(93) + cpx(6) + ol(1) + ox(tr)	0.3	−3.73	0.232	0.226	
(6-4)	0.70	0.170	−8.82	0.51	gl(87) + cpx(11) + ol(2) + ox(tr)	0.1	−9.88	0.292	0.222	

Water activity (aH_2O) calculated from H_2O_{melt} using the Burnham (1979) model and melt compositions from Tables 3 and 4; fH_2 experimentally determined as explained in text; logfO_2 calculated from fH_2 and experimental fH_2O (see text); ΔNNO = logfO_2 − logfO_2 of the NNO buffer calculated at the given T; tr: occurrence in trace amounts (<0.5 wt.%); (?): presence of oxide not confirmed due to its very small size. Phase proportions are calculated by mass balance; gl, glass; cpx, clinopyroxene; ol, olivine; pl, plagioclase; ox, Fe-oxide; qc, quench crystals. Iron loss (ΔFeO) is calculated as $100 \cdot (FeO_{calc} - FeO_{st.\ glass})/FeO_{st.\ glass}$. FeO_{calc} and $\sum R^2$ are obtained from the mass balance calculations. H_2O concentrations in glass estimated with the "by-difference" method (Devine et al., 1995); numbers in brackets indicate water concentrations measured by FTIR. $K_d^{Fe-Mg}{}_{cpx-liq} = (Fe/Mg)_{cpx}/(Fe/Mg)_{liq}$; $K_d^{Fe-Mg}{}_{ol-liq} = (Fe/Mg)_{ol}/(Fe/Mg)_{liq}$; $K_d^{Ca-Na}{}_{pl-liq} = (Ca/Na)_{pl}/(Ca/Na)_{liq}$. For cpx, the Kd is calculated with FeO = FeO_{tot}.

3.5. Analytical techniques

Experimental charges were mounted in epoxy resin, polished and examined with a scanning electron microscope (SEM-EDS) for the identification of mineral phases, textural observations, and to check for quench crystallization. An electron microprobe (EPMA) was used for the determination of phase compositions. Analytical conditions were as follows: (i) SEM-EDS (Oxford LEO 440 at University of Palermo): acceleration voltage 20 kV, beam current 600 pA; (ii) EMP (Cameca SX50 and SX Five at University of Orléans: acceleration voltage 15 kV, sample current 6 nA). A focused beam was used for crystals whilst for glasses a defocused beam of 10 μm was adopted to minimize alkali migration.

The water contents of the experimental glasses were determined using the "by-difference" method (Devine et al., 1995). For each analytical session, a calibration curve was established using a set of secondary basaltic glass standards of known H_2O and alkali contents (PST-9, Di Carlo et al., 2006). This method yields an uncertainty typically from ±0.5 to ±1.0 wt.% H_2O depending on glass analytical totals. These estimates were checked against H_2O concentration measurements by FTIR on experimental glasses from 4 near-liquidus charges. The FTIR absorption spectra were acquired on a Hyperion 2000 Bruker FTIR (at University of Palermo). Measurements were performed on doubly-polished experimental glasses employing a Globar source, a KBr beam splitter and an HgCdTe detector. 256 scans were accumulated for each spectrum with a resolution of 2 cm^{-1}. The water content was derived from the Beer–Lambert law using the band at 3550 cm^{-1} (H_2O_{tot}) and a molar extinction coefficient (ε) of 43.96 L mol^{-1} cm^{-1} (Mercier et al., 2010). The density of the starting volatile-free glass (2718 ± 11 kg m^{-3}) was measured by using a Mettler Toledo Density kit and a high precision balance at University of Orléans. For the volatile-bearing experimental glasses, densities were calculated using an iterative method (Pichavant et al., 2009).

4. Experimental results

The experiments (24 charges in total) are divided into two groups: (i) isobaric experiments at 150 MPa and (ii) isothermal experiments at 1150 °C. The data used for the construction of the phase diagrams are detailed in Table 2. In this study, melt H_2O contents were varied from 0.7 to 3.5 wt.% (Table 2). The FTIR data are in good agreement with the H_2O concentrations estimated with the "by difference" method (Table 2), which validates our "by-difference" estimations of the glass H_2O content. The oxygen fugacity is in the range NNO + 0.2 to +1.9 (Table 2), encompassing the range of fO_2 estimated for the La Sommata basalt. There is no systematic difference in fO_2 between the isobaric and isothermal experiments.

4.1. Attainment of equilibrium, quench crystallization and iron loss

Run duration ranged between 20 to 26 h, which is considered long enough to achieve crystal-melt equilibrium in basaltic compositions under our P-T conditions (e.g. Di Carlo et al., 2006; Barclay and Carmichael, 2004). This is witnessed by a number of textural and chemical features, among which: (i) the shapes of crystals: clinopyroxene, olivine and plagioclase crystals have euhedral and equant shapes suggesting growth at small degrees of undercooling (Muncill and Lasaga, 1987); (ii) uniform crystal distributions in experimental products (neither crystal settling nor seriate crystal sizes were observed); (iii) homogeneity of glass composition throughout each charge; (iv) consistent changes of the melt composition with T, P, H_2O_{melt}; (v) low residuals of the mass balance calculations (Table 2); (vi) near-equilibrium mineral-melt partition coefficients. The Fe–Mg crystal-liquid distribution coefficient ($K_d^{Fe-Mg}{}_{cpx-liq}$, Table 2) is 0.29 ± 0.05 for clinopyroxene-liquid (calculated using all Fe as FeO_{tot} in both crystal and melt), close to values in recent crystallization experiments on basaltic compositions (0.25, Grove et al., 1997; 0.31, Di Carlo et al., 2006). For olivine-liquid, the distribution coefficient ($K_d^{Fe-Mg}{}_{ol-liq}$) is 0.25 ± 0.03 using melt FeO calculated from Kress and Carmichael (1991), which is slightly lower (but close) than the expected range for olivine in basaltic liquids (0.30, Grove et al., 1997; 0.33, Pichavant et al., 2002; 0.28, Barclay and Carmichael, 2004; 0.36, Di Carlo et al., 2006; 0.32, Pichavant and Macdonald, 2007). For plagioclase, the Na-Ca crystal-liquid distribution coefficient determined for charge #5-5 (Table 2, $K_d^{Na-Ca}{}_{plag-liq} = 1.5$) is in agreement with experimental data under similar P-T conditions and H_2O_{melt} (Di Carlo et al., 2006).

The use of the fast quench device dramatically reduced the importance of quench crystallization (Di Carlo et al., 2006). Nevertheless, SEM observations revealed the presence of quench phases growing on Fe-oxides in some charges (runs #3-1, #3-2, #3-3, #5-1, #52, Table 2). Glass in charge #5-1 is anomalously low in MgO and K_2O, and the other charges with quench crystals are characterized by $K_d^{Fe-Mg}{}_{cpx-liq}$ and $K_d^{Fe-Mg}{}_{ol-liq}$ slightly lower than average (Table 2).

The amount of Fe loss was obtained from the mass balance calculations and is expressed as the relative difference between the FeO_{tot} of the starting glass and that calculated by summing FeO_{tot} concentrations for all phases present in the charge (ΔFeO, Table 2). The resulting average value is −3.8%, whilst the range is −0.3 to −11.5%. Six on a total of 24 charges have >5% Fe loss and one >10%. We conclude that Fe loss was kept to a low level in our experiments.

4.2. Mineral phases

Mineral phases encountered include a Fe-oxide, clinopyroxene, olivine and plagioclase. Crystal sizes rarely exceeded 20 μm. Olivine reached sizes ~100 μm in near-liquidus charges, but is generally smaller when the proportion of crystals increases (Fig. 5). Exceptionally large plagioclase crystals (~100 μm) were found in one charge (#5-5, Table 2). Fe-oxides have very small sizes (less than 10 μm and as small as 1–2 μm) which make their identification difficult, especially in charges with low melt H_2O content (#2-4, 3-5, 6-4; Table 2; Fig. 5).

4.3. Phase relationships at 150 MPa

The isobaric phase equilibrium diagram is shown in Fig. 6. Solid lines represent mineral saturation curves constructed using the data set from Table 2. All saturation curves have strongly negative slopes, as found in previous studies (Di Carlo et al., 2006). Over all the investigated T-H_2O

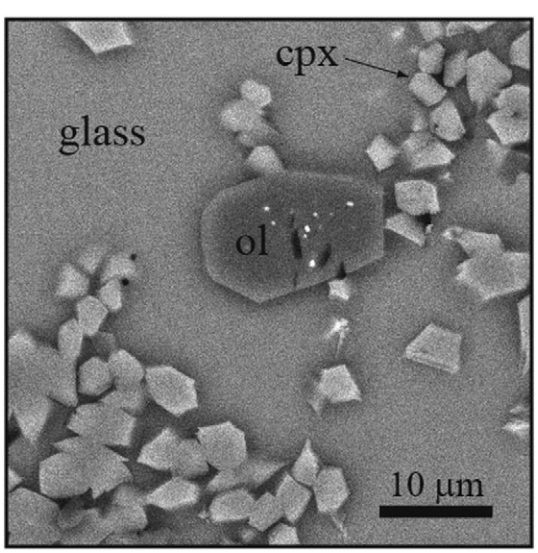


Fig. 5. Back-scattered electron microphotograph of experimental charge #2-4 illustrating the crystallization of a cotectic (Cpx + Ol co-saturated) assemblage. Experimental conditions in Table 2. Clinopyroxene (cpx) is Fs_9 and olivine (ol) Fo_{89} (data in Table 3). Notice the presence of small Fe-oxide crystals included in olivine and the lack of quench crystals.

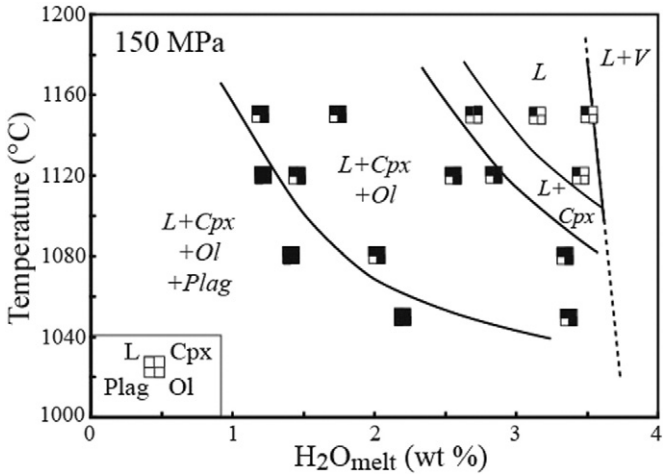


Fig. 6. Experimentally determined T-H_2O_{melt} phase diagram for Som-1 at P = 150 MPa. Experimental data in Table 2. Squares give conditions of experimental charges and types of phase assemblages encountered. Open square: phase is absent; filled square: phase is present. Note that Fe-oxide occurs in most charges although its presence could not be confirmed in all because of its small size. L: liquid; Cpx: clinopyroxene; Ol: olivine; Plag: plagioclase. All charges include a fluid phase (see text). Pure H_2O vapour is designated as V and the L — L + V phase boundary is the H_2O solubility curve.

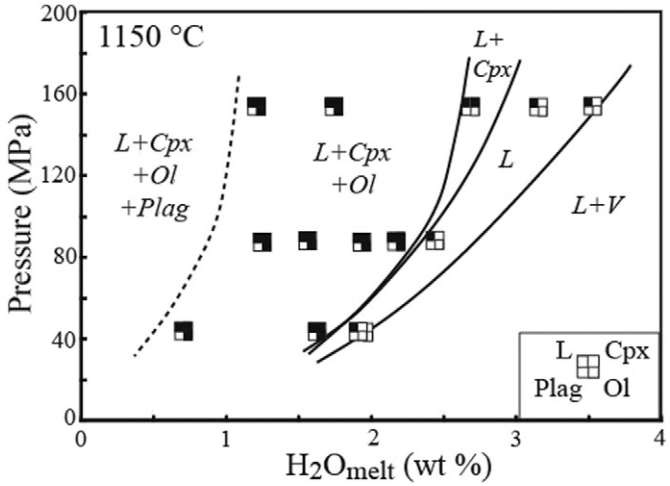


Fig. 7. Experimentally determined P-H_2O_{melt} phase diagram for Som-1 at T = 1150°C. Experimental data in Table 2. Squares give conditions of experimental charges and types of phase assemblages encountered. Open square: phase is absent; filled square: phase is present. Note that Fe-oxide occurs in most charges although its presence could not be confirmed in all because of its small size. L: liquid; Cpx: clinopyroxene; Ol: olivine; Plag: plagioclase. All charges include a fluid phase (see text). Pure H_2O vapour is designated as V and the L — L + V phase boundary is the H_2O solubility curve. The location of the plagioclase saturation curve (dashed) is estimated.

section, Fe-oxide is the liquidus phase, followed by clinopyroxene, olivine, and plagioclase. However, Fe-oxide was not positively detected in all charges because of its very small size. There are also differences in fO_2 between charges that could influence Fe-oxide stability. Clinopyroxene and olivine crystallize very close to each other (Fig. 6); only one charge (#2-3, Table 2) demonstrates that clinopyroxene precedes olivine in the crystallization sequence. The H_2O content of cotectic (olivine- and clinopyroxene-saturated) liquids increases with decreasing temperature from 2.7 wt.% (1150 °C), 2.9 wt.% (1120 °C) to 3.3 wt.% (1080 °C). The melt H_2O content at plagioclase saturation decreases from 2.8 wt.% (1050 °C) to about 1.2 wt.% (1120 °C). Conditions of H_2O-saturation are defined by the CO_2-free charges #2-1, 5-1, and 8-1. For these charges, the melt H_2O concentrations (some being duplicated by FTIR measurements) range between 3.3 and 3.6 wt.% H_2O at 1150 °C (Table 2). These values are in good agreement with H_2O solubilities calculated for the specific melt compositions with the model of Burnham (1979).

4.4. Phase relationships at 1150 °C

The isothermal phase diagram is shown in Fig. 7. Three pressure conditions were explored at 1150 °C: 150, ~100 and ~50 MPa. In this representation, saturation curves have positive slopes. Our data do not reveal any change in the sequence of crystallization with pressure but the clinopyroxene and olivine saturation curves become closer to each other with decreasing pressure (see below). With decreasing melt H_2O content, Fe-oxide is followed by clinopyroxene, olivine and plagioclase. Clinopyroxene and olivine saturation curves have steep slopes and are very close to each other. The H_2O content of cotectic liquids decreases with decreasing pressure from about 2.4 wt.% (150 MPa), 2.2 wt.% (100 MPa) to 1.6 wt.% (50 MPa). It is worth emphasizing that plagioclase was not encountered at 1150 °C. Therefore, the plagioclase saturation curve (Fig 7) is estimated. The vapor-saturation curve is defined by the charges #2-1, 3-1 and 61 which have melt H_2O concentrations in close agreement with solubilities calculated with the model of Burnham (1979).

4.5. Proportions and compositions of crystals

Proportions of crystalline phases range from ~0 (several charges are above the liquidus, Table 2) to 54% (charge #8-3, Table 2), generally increasing with decreasing temperature, pressure and melt H_2O content. Clinopyroxene is the most abundant mineral phase (up to 50 wt.%, in charge #8-3), followed by Fe-oxide (up to 5 wt.%) and olivine (up to 3 wt.%). Plagioclase is never very abundant, being present only at low levels (<1 wt.%).

The Fe-oxide proportion tends to decrease with increasing crystallinity. Because of its small size, Fe-oxide could not be analyzed nor unequivocally detected in all charges. This phase is a Ti-, Al-, Mg-, and Cr-bearing magnetite (Tables 3, 4). TiO_2 and Al_2O_3, which are positively correlated, range from 0.58 to 3.08 and 4.39 to 10.92 wt.%, respectively, both slightly increasing with increasing crystallinity. However, there is also an influence of fO_2: increasing fO_2 decreases the TiO_2 and Al_2O_3 concentration in Fe-oxide. The MgO concentration ranges from 12.4 wt.% at near-liquidus conditions (T = 1150 °C) to 7.23 wt.% at lower temperatures (T = 1050 °C), and is positively correlated with fO_2. Fe-oxide is relatively Cr-rich (6.88 wt.% Cr_2O_3) at near-liquidus conditions, but the Cr concentration drops to below detection at lower temperatures. It is emphasized that chromite compositions typical of the basaltic phenocryst assemblage have not been found in experimental products due to the low Cr concentration of the starting material (~250 ppm). This is consistent with our previous conclusion that Som-1 bulk rock does not correspond exactly to an end-member primitive liquid despite near-primary compositions (olivine, chromite, clinopyroxene, melt inclusions) being present.

Clinopyroxene composition (Tables 3, 4) ranges from diopside ($Wo_{47}En_{46}Fs_7$, X_{Mg} = 0.87) to augite ($Wo_{44}En_{40}Fs_{16}$, X_{Mg} = 0.72). TiO_2, Al_2O_3 and Cr_2O_3 contents range from 0.22 to 0.73, 2.72 to 7.17 and from 0 to 0.71 wt.%, respectively. With progressive crystallization, X_{Mg} decreases, Wo slightly decreases, TiO_2 and Al_2O_3 increase and Cr_2O_3 drops to below detection. The Ca (apfu) in pyroxene shows a weak positive correlation with the melt H_2O content.

Olivine has Fo between 78 and 92, 0.49 ± 0.16 wt.% CaO and 0.3 ± 0.08 wt.% MnO. The Fo content of experimental olivine is governed by two parameters, fO_2 (or ΔNNO) and the crystallinity of the charge (or the MgO content of the melt). Fo increases with increasing fO_2 and decreases with the proportion of crystals, this latter variable being itself determined by the experimental parameters (P, T, H_2O_{melt}). The most Fo-rich olivines correspond to the most oxidized charges (ΔNNO ~ 1.5) with crystallinities between 10 and 20% (charges #5-2, #3-2, Table 2). Crystal-poor (<10%) charges with ΔNNO between

Table 3
SOM-1 experimental compositions at 150 MPa.

Charge	Phase	SiO_2	TiO_2	Al_2O_3	FeO_t	MnO	MgO	CaO	Na_2O	K_2O	P_2O_5	Cr_2O_3	Total	Fo	En	Fs	An	Mg#	Usp	CaO/Al_2O_3
SOM-1	Startgl(n = 179)	48.56(0.3)	0.72(0.1)	12.41(0.2)	10.03(0.1)	0.21(0.3)	8.61(0.1)	12.72(0.2)	2.14(0.1)	2.24(0.1)	0.39(0.1)	–	98.02	–	–	–	–	0.60	–	1.03
2-1	gl(n = 8)	46.75(0.2)	0.71(0.1)	12.21(0.1)	9.81(0.3)	0.20(0.1)	8.31(0.1)	11.99(0.2)	2.07(0.1)	2.04(0.1)	0.42(0.2)	0.00(0.0)	94.51	–	–	–	–	0.60	–	0.98
2-2	gl(n = 5)	47.19(0.1)	0.69(0.1)	12.22(0.1)	9.20(0.3)	0.19(0.0)	8.30(0.2)	12.2(0.2)	2.07(0.1)	2.13(0.1)	0.46(0.0)	0.00(0.0)	94.66	–	–	–	–	0.62	–	1.00
2-3	gl(n = 5)	47.26(0.3)	0.78(0.1)	13.18(0.2)	10.00(0.2)	0.16(0.1)	7.86(0.1)	11.42(0.3)	2.29(0.1)	2.33(0.1)	0.48(0.1)	0.00(0.0)	95.76	–	–	–	–	0.58	–	0.87
	cpx(n = 3)	51.75(0.1)	0.22(0.1)	2.67(0.0)	5.59(0.1)	0.00(0.0)	16.77(0.1)	21.87(0.2)	0.20(0.0)	0.01(0.0)	0.10(0.0)	0.00(0.0)	99.18	–	47	9	–	0.84	–	–
2-4	gl(n = 11)	48.51(0.3)	0.85(0.1)	14.91(0.3)	9.91(0.3)	0.2(0.1)	6.38(0.3)	10.39(0.4)	2.66(0.1)	2.77(0.1)	0.46(0.2)	0.00(0.0)	97.04	–	–	–	–	0.53	–	0.70
	cpx(n = 3)	50.16(0.2)	0.41(0.0)	4.60(0.2)	5.36(0.2)	0.17(0.1)	15.15(0.3)	21.91(0.3)	0.32(0.0)	0.13(0.0)	0.21(0.0)	0.00(0.0)	98.42	–	45	9	–	0.83	–	–
	ol(n = 3)	40.39(0.2)	0.00(0.1)	0.59(0.1)	10.37(0.1)	0.23(0.0)	45.1(0.3)	0.87(0.3)	0.09(0.0)	0.14(0.0)	0.01(0.0)	0.00(0.0)	97.80	89	–	–	–	–	–	–
2-5	gl(n = 8)	48.49(0.4)	0.86(0.1)	15.48(0.1)	10.08(0.3)	0.22(0.1)	5.68(0.1)	10.01(0.2)	2.75(0.1)	2.85(0.1)	0.58(0.1)	0.00(0.0)	97.00	–	–	–	–	0.50	–	0.65
	cpx(n = 3)	50.07(0.2)	0.46(0.0)	4.95(0.2)	7.79(0.2)	0.05(0.0)	15.22(0.3)	21.53(0.2)	0.32(0.1)	0.14(0.0)	0.00(0.0)	0.00(0.0)	100.52	–	44	12	–	0.78	–	–
	ol(n = 2)	39.49(0.1)	0.00(0.0)	0.06(0.0)	17.00(0.2)	0.25(0.2)	44.74(0.3)	0.48(0.3)	0.00(0.0)	0.02(0.0)	0.00(0.0)	0.00(0.0)	102.04	82	–	–	–	–	–	–
5-1	gl(n = 6)	47.39(1.4)	0.73(0.0)	13.19(0.3)	8.90(0.6)	0.14(0.1)	6.59(1.8)	12.45(1.8)	2.19(0.2)	1.54(1.0)	0.48(0.0)	0.00(0.0)	93.59	–	–	–	–	0.57	–	0.94
	ox(n = 2)	0.13(0.0)	0.58(0.1)	4.39(0.2)	70.44(0.5)	0.00(0.0)	8.41(0.3)	0.58(0.2)	0.99(0.1)	0.00(0.0)	0.00(0.0)	3.05(0.2)	88.56	–	–	–	–	–	1	–
5-2	gl(n = 3)	48.55(0.2)	0.77(0.1)	15.01(0.2)	8.67(0.3)	0.19(0.1)	5.83(0.1)	11.21(0.4)	2.55(0.2)	2.38(0.1)	0.49(0.1)	0.00(0.0)	95.65	–	–	–	–	0.55	–	0.75
	cpx(n = 3)	50.40(1.0)	0.23(0.0)	3.16(0.5)	4.61(0.1)	0.12(0.0)	16.16(0.3)	22.76(0.1)	0.19(0.0)	0.04(0.0)	0.31(0.1)	0.00(0.0)	98.12	–	46	7	–	0.86	–	–
	ol(n = 2)	40.28(0.1)	0.00(0.01)	0.00(0.0)	8.08(0.0)	0.27(0.1)	50.02(0.2)	0.37(0.1)	0.00(0.0)	0.02(0.0)	0.10(0.0)	0.01(0.0)	99.25	92	–	–	–	–	–	–
	ox(n = 2)	0.27(0.0)	1.17(0.1)	5.11(0.3)	70.07(0.3)	0.64(0.1)	7.61(0.6)	0.49(0.0)	1.04(0.1)	0.04(0.0)	0.00(0.0)	2.75(0.2)	89.19	–	–	–	–	–	3	–
5-3	gl(n = 5)	49.50(1.0)	0.75(0.0)	15.05(0.7)	8.90(0.3)	0.20(0.1)	5.70(0.5)	11.02(1.0)	2.65(0.3)	2.55(0.4)	0.48(0.1)	0.00(0.0)	94.29	–	–	–	–	0.51	–	0.73
	cpx(n = 5)	49.06(0.5)	0.47(0.1)	5.88(1.1)	7.47(0.4)	0.15(0.1)	14.9(0.8)	21.32(0.9)	0.39(0.3)	0.35(0.2)	0.40(0.0)	0.06(0.0)	100.44	–	44	10	–	0.82	–	–
	ol(n = 3)	40.15(0.4)	0.03(0.1)	0.02(0.0)	9.01(0.1)	0.35(0.1)	47.88(0.7)	0.40(0.1)	0.00(0.0)	0.02(0.0)	0.11(0.1)	0.01(0.0)	97.97	90	–	–	–	–	–	–
	ox(n = 2)	0.01(0.1)	1.60(0.2)	6.16(0.2)	70.05(0.6)	0.56(0.1)	7.85(0.3)	0.42(0.0)	0.20(0.0)	0.08(0.0)	0.30(0.1)	0.99(0.1)	88.23	–	–	–	–	–	4	–
5-4	gl(n = 4)	50.08(0.4)	0.75(0.1)	16.68(0.2)	8.93(0.3)	0.19(0.1)	5.21(0.1)	8.64(0.2)	3.14(0.2)	3.26(0.1)	0.62(0.0)	0.00(0.0)	97.5	–	–	–	–	0.51	–	0.52
	cpx(n = 3)	48.12(0.8)	0.53(0.8)	5.60(0.6)	6.38(0.6)	0.21(0.1)	14.8(0.2)	21.81(0.2)	0.25(0.0)	0.07(0.0)	0.40(0.0)	0.05(0.0)	98.21	–	44	10	–	0.81	–	–
	ol(n = 4)	40.41(0.3)	0.02(0.0)	0.01(0.0)	14.68(0.2)	0.35(0.1)	46.63(0.3)	0.34(0.0)	0.00(0.0)	0.02(0.0)	0.00(0.0)	0.00(0.0)	102.45	85	–	–	–	–	–	–
	ox(n = 2)	0.16(0.0)	2.36(0.1)	7.38(0.2)	69.89(0.5)	0.31(0.1)	7.23(0.3)	0.43(0.1)	0.00(0.0)	0.14(0.1)	0.30(0.1)	1.00(0.1)	89.2	–	–	–	–	–	6	–
5-5	gl(n = 3)	49.19(0.1)	0.90(0.1)	16.79(0.3)	10.04(0.4)	0.23(0.1)	4.48(0.1)	8.58(0.2)	3.21(0.1)	3.27(0.2)	0.51(0.1)	0.00(0.0)	97.19	–	–	–	–	0.44	–	0.51
	cpx(n = 5)	49.72(0.1)	0.60(0.1)	6.25(0.0)	6.80(0.1)	0.25(0.0)	14.06(0.1)	21.17(0.2)	0.52(0.2)	0.42(0.2)	0.44(0.0)	0.10(0.0)	98.53	–	42	12	–	0.79	–	–
	ol(n = 3)	38.91(0.2)	0.07(0.0)	0.00(0.0)	15.27(0.0)	0.47(0.1)	42.03(0.4)	0.49(0.0)	0.00(0.0)	0.05(0.0)	0.17(0.0)	0.03(0.0)	97.48	83	–	–	–	–	–	–
	pl(n = 3)	49.94(0.2)	0.02(0.0)	33.08(0.4)	0.78(0.0)	0.00(0.0)	0.00(0.0)	12.59(0.2)	9.00(0.3)	0.48(0.1)	0.00(0.0)	0.00(0.0)	100.05	–	–	–	67	–	–	–
8-1	gl(n = 5)	48.32(3.8)	0.66(0.1)	14.78(1.4)	6.76(2.0)	0.10(0.1)	4.22(3.7)	9.10(2.5)	2.34(0.7)	2.63(1.64)	0.51(0.2)	0.00(0.0)	89.43	–	–	–	–	0.53	–	0.62
	cpx(n = 3)	49.9(0.7)	0.57(0.1)	5.38(0.7)	6.95(0.5)	0.13(0.1)	14.93(0.7)	21.89(0.6)	0.39(0.1)	0.22(0.1)	–	–	–	–	43	11	–	0.79	–	–
	ox(n = 2)	0.01(0.1)	1.60(0.2)	6.16(0.2)	70.05(0.6)	0.56(0.1)	7.85(0.3)	0.42(0.0)	0.20(0.0)	0.08(0.0)	0.3(0.1)	0.99(0.1)	88.23	–	–	–	–	–	4	–
8-2	gl(n = 3)	52.56(0.4)	0.69(0.0)	16.78(0.1)	6.45(0.5)	0.16(0.1)	3.31(0.1)	6.42(0.1)	3.68(0.1)	4.14(0.2)	0.67(0.1)	0.00(0.0)	94.87	–	–	–	–	0.48	–	0.38
	cpx(n = 3)	49.22(0.6)	0.70(0.1)	6.65(0.7)	8.45(0.3)	0.13(0.1)	13.83(0.5)	20.51(0.4)	0.53(0.1)	0.30(0.1)	0.13(0.0)	0.00(0.0)	100.44		42	14	–	–	–	–
	ol(n = 3)	39.8(0.6)	0.07(0.1)	0.57(0.1)	16.17(0.1)	0.46(0.0)	44.4(0.4)	0.71(0.3)	0.06(0.0)	0.08(0.1)	0.10(0.0)	0.00(0.0)	102.42	83	–	–	–	–	–	–
	ox(n = 2)	1.33(0.1)	1.29(0.1)	6.42(0.2)	77.99(0.4)	0.40(0.0)	9.02(0.3)	1.19(0.5)	1.21(0.5)	0.00(0.0)	0.43(0.1)	0.01(0.0)	–	–	–	–	–	–	2	–
8-3	gl(n = 3)	52.17(0.1)	0.74(0.1)	16.46(0.2)	7.16(0.2)	0.17(0.1)	3.06(0.5)	5.93(0.3)	3.93(0.1)	5.13(0.3)	0.83(0.1)	0.00(0.0)	95.57	–	–	–	–	0.43	–	0.36
	cpx(n = 4)	49.05(0.5)	0.67(0.0)	7.16(0.5)	8.99(0.5)	0.23(0.1)	12.69(0.3)	19.55(0.3)	0.83(0.1)	0.64(0.1)	0.10(0.0)	0.00(0.0)	99.93	–	40	16	–	0.72	–	–
	ol(n = 3)	40.08(0.2)	0.1(0.1)	0.67(0.3)	19.11(0.3)	0.23(0.1)	38.6(0.1)	0.42(0.2)	0.98(0.0)	0.04(0.0)	0.00(0.0)	0.00(0.0)	100.22	78	–	–	–	–	–	–
	ox(n = 2)	1.67(0.2)	3.08(0.3)	10.92(0.4)	73.49(0.7)	0.66(0.0)	7.99(0.5)	0.65(0.0)	1.30(0.1)	0.26(0.0)	0.00(0.0)	0.00(0.0)	–	–	–	–	–	–	9	–
7-5	gl(n = 5)	50.13(0.4)	0.56(0.1)	15.74(0.5)	5.53(0.5)	0.05(0.1)	4.17(0.4)	9.18(0.9)	1.8(0.4)	2.89(0.2)	0.53(0.1)	0.00(0.0)	90.57	–	–	–	–	0.57	–	0.58
	cpx(n = 3)	49.52(0.5)	0.73(0.1)	6.99(1.0)	7.3(0.5)	0.15(0.1)	13.87(0.9)	21.22(1.0)	0.53(0.2)	0.36(0.2)	0.00(0.0)	0.00(0.0)	100.67	–	42	12	–	0.77	–	–
	ol(n = 3)	41.09(0.4)	0.02(0.0)	0.02(0.1)	10.66(0.4)	0.35(0.1)	50.32(0.7)	0.22(0.0)	0.00(0.0)	0.02(0.0)	0.00(0.0)	0.00(0.0)	102.7	89	–	–	–	–	–	–
	ox(n = 2)	7.07(0.5)	2.05(0.7)	7.01(0.8)	70.01(0.9)	0.6(0.0)	8.05(0.8)	2.85(0.7)	1.51(0.5)	0.3(0.1)	0.09(0.0)	0.00(0.0)	–	–	–	–	–	–	6	–
7-6	gl(n = 6)	52.18(0.3)	0.64(0.1)	17.09(0.3)	6.01(0.3)	0.19(0.1)	3.39(0.1)	6.55(0.3)	3.62(0.2)	4.01(0.2)	0.66(0.1)	0.00(0.0)	94.33	–	–	–	–	0.50	–	0.38
	cpx(n = 3)	48.92(0.3)	0.63(0.1)	7.05(0.3)	7.61(0.3)	0.15(0.1)	13.63(0.3)	20.33(0.4)	0.62(0.1)	0.39(0.1)	0.00(0.0)	0.00(0.0)	99.33	–	42	13	–	0.76	–	–
	ol(n = 3)	39.47(0.2)	0.09(0.0)	0.53(0.4)	16.34(0.7)	0.39(0.1)	44.18(0.8)	0.63(0.2)	0.04(0.1)	0.07(0.1)	0.00(0.0)	0.00(0.0)	101.74	83	–	–	–	–	–	–
	ox(n = 2)	5.94(0.6)	1.53(0.3)	7.05(0.8)	73.37(0.9)	0.3(0.0)	7.94(0.5)	1.97(0.4)	1.44(0.3)	0.33(0.1)	0.00(0.0)	0.00(0.0)	–	–	–	–	–	–	4	–

Compositions of experimental glasses and minerals analyzed at EPMA. SOM-1, starting glass; other abbreviations as in Table 2. CaO/Al_2O_3 is calculated for the glass phase. In brackets standard deviation with n = number of analyses. All Fe as FeO_{tot}. Wo = 100 * Ca/(Mg + Fe + Ca), En = 100 * Mg/(Mg + Fe + Ca) and Fs = 100 * Fe/(Mg + Fe + Ca) with Fe = FeO_t; An = 100 * Ca/(Ca + Na + K); Ab = 100 * Na/(Ca + Na + K).

Table 4
SOM-1 experimental compositions at 1150 °C.

Charge	Phase	SiO_2	TiO_2	Al_2O_3	FeO_t	MnO	MgO	CaO	Na_2O	K_2O	P_2O_5	Cr_2O_3	Tot	Fo	En	Fs	An	Mg#	Usp	CaO/Al_2O_3
SOM-1	Startgl(n = 179)	48.56(0.3)	0.72(0.1)	12.41(0.2)	10.03(0.1)	0.21(0.3)	8.61(0.1)	12.72(0.2)	2.14(0.1)	2.24(0.1)	0.39(0.1)	–	98.02	–	–	–	–	0.60	–	1.03
2-1	gl(n = 8)	46.75(0.2)	0.71(0.1)	12.21(0.1)	9.81(0.3)	0.2(0.1)	8.31(0.1)	11.99(0.2)	2.07(0.1)	2.04(0.1)	0.42(0.2)	0.00(0.0)	94.51	–	–	–	–	0.60	–	0.98
2-2	gl(n = 5)	47.19(0.1)	0.69(0.1)	12.22(0.1)	9.2(0.3)	0.19(0.0)	8.3(0.2)	12.2(0.2)	2.07(0.1)	2.13(0.1)	0.46(0.0)	0.00(0.0)	94.66	–	–	–	–	0.62	–	1.00
2-3	gl(n = 5)	47.26(0.3)	0.78(0.1)	13.18(0.2)	10.00(0.2)	0.16(0.1)	7.86(0.1)	11.42(0.3)	2.29(0.1)	2.33(0.1)	0.48(0.1)	0.00(0.0)	95.76	–	–	–	–	0.58	–	0.87
	cpx(n = 3)	51.75(0.1)	0.22(0.1)	2.67(0.0)	5.59(0.1)	0.00(0.0)	16.77(0.1)	21.87(0.2)	0.20(0.0)	0.01(0.0)	0.10(0.0)	0.00(0.0)	99.18	–	47	9	–	0.84	–	–
2-4	gl(n = 11)	48.51(0.3)	0.85(0.1)	14.91(0.3)	9.91(0.3)	0.2(0.1)	6.38(0.3)	10.39(0.4)	2.66(0.1)	2.77(0.1)	0.46(0.2)	0.00(0.0)	97.04	–	–	–	–	0.53	–	0.70
	cpx(n = 3)	50.16(0.2)	0.41(0.0)	4.6(0.2)	5.36(0.2)	0.17(0.1)	15.15(0.3)	21.91(0.3)	0.32(0.0)	0.13(0.0)	0.21(0.0)	0.00(0.0)	98.42	–	45	9	–	0.83	–	–
	ol(n = 3)	40.39(0.2)	0.00(0.1)	0.59(0.1)	10.37(0.1)	0.23(0.0)	45.1(0.3)	0.87(0.3)	0.09(0.0)	0.14(0.0)	0.01(0.0)	0.00(0.0)	97.80	89	–	–	–	–	–	–
2-5	gl(n = 8)	48.49(0.4)	0.86(0.1)	15.48(0.1)	10.08(0.3)	0.22(0.1)	5.68(0.1)	10.01(0.2)	2.75(0.1)	2.85(0.1)	0.58(0.1)	0.00(0.0)	97.00	–	–	–	–	0.50	–	0.65
	cpx(n = 3)	50.07(0.2)	0.46(0.0)	4.95(0.2)	7.79(0.2)	0.05(0.0)	15.22(0.3)	21.53(0.2)	0.32(0.1)	0.14(0.0)	0.00(0.0)	0.00(0.0)	100.52	–	44	12	–	–	–	–
	ol(n = 2)	39.49(0.1)	0.00(0.0)	0.06(0.0)	17.00(0.2)	0.25(0.2)	44.74(0.3)	0.48(0.3)	0.00(0.0)	0.02(0.0)	0.00(0.0)	0.00(0.0)	102.04	82	–	–	–	–	–	–
3-1	gl(n = 3)	46.61(0.2)	0.7(0.1)	12.25(0.1)	9.84(0.2)	0.17(0.1)	8.2(0.2)	11.54(0.2)	2.05(0.2)	2.32(0.1)	0.43(0.1)	0.00(0.0)	94.11	–	–	–	–	0.60	–	0.94
3-2	gl(n = 3)	47.31(0.2)	0.66(0.1)	12.65(0.1)	9.89(0.3)	0.19(0.1)	7.64(0.1)	11.21(0.3)	2.43(0.2)	2.37(0.2)	0.44(0.1)	0.00(0.0)	94.79	–	–	–	–	0.58	–	0.89
	cpx(n = 2)	49.76(0.1)	0.45(0.0)	4.04(0.0)	5.02(0.1)	0.11(0.1)	15.87(0.0)	23.24(0.3)	0.18(0.1)	0.04(0.0)	0.4(0.0)	0.53(0.2)	99.64	–	45	8	–	–	–	–
	ol(n = 2)	40.83(0.1)	0.05(0.0)	0.00(0.0)	7.65(0.3)	0.27(0.0)	50.99(0.6)	0.43(0.0)	0.00(0.0)	0.01(0.0)	0.26(0.0)	0.01(0.0)	100.49	92	–	–	–	–	–	–
	ox(n = 2)	0.77(0.0)	1.57(0.2)	5.32(0.2)	70.85(0.5)	0.57(0.1)	12.37(0.2)	2.18(0.1)	0.00(0.0)	0.00(0.0)	0.00(0.0)	6.88(0.3)	100.52	–	–	–	–	–	2	–
3-3	gl(n = 3)	47.8(0.1)	0.62(0.1)	13.07(0.1)	9.98(0.3)	0.20(0.1)	7.01(0.2)	10.91(0.3)	2.75(0.2)	2.55(0.1)	0.46(0.1)	0.00(0.0)	95.35	–	–	–	–	0.56	–	0.83
	cpx(n = 2)	50.23(0.1)	0.35(0.0)	3.62(0.1)	4.91(0.1)	0.16(0.1)	16.26(0.0)	22.55(0.0)	0.19(0.0)	0.06(0.0)	0.39(0.0)	0.71(0.0)	99.43	–	46	8	–	0.86	–	–
	ol(n = 2)	40.56(0.1)	0.04(0.0)	0.00(0.0)	8.40(0.4)	0.30(0.0)	49.7(0.1)	0.47(0.0)	0.00(0.0)	0.03(0.0)	0.13(0.1)	0.01(0.0)	99.65	91	–	–	–	–	–	–
3-4	gl(n = 5)	48.41(0.3)	0.8(0.0)	14.63(0.2)	10.3(0.3)	0.19(0.1)	6.2(0.2)	10.65(0.3)	2.47(0.1)	2.42(0.2)	0.47(0.1)	0.00(0.0)	96.55	–	–	–	–	0.52	–	0.73
	cpx(n = 2)	49.7(0.1)	0.47(0.1)	4.39(0.3)	7.46(0.1)	0.11(0.0)	15.2(0.1)	21.32(0.2)	0.28(0.0)	0.00(0.0)	0.00(0.0)	0.00(0.0)	98.93	–	44	12	–	0.78	–	–
	ol(n = 2)	40.21(0.2)	0.00(0.0)	0.00(0.0)	14.42(0.2)	0.22(0.1)	46.44(0.2)	0.39(0.1)	0.00(0.0)	0.00(0.0)	0.00(0.0)	0.00(0.0)	101.68	85	–	–	–	–	–	–
3-5	gl(n = 5)	48.88(0.4)	0.82(0.1)	15.37(0.1)	9.85(0.5)	0.18(0.1)	5.74(0.3)	10.46(0.4)	2.84(0.1)	2.75(0.1)	0.57(0.1)	0.00(0.0)	97.45	–	–	–	–	0.51	–	0.68
	cpx(n = 2)	50.21(0.2)	0.45(0.1)	5.5(0.2)	7.38(0.2)	0.06(0.0)	14.23(0.1)	20.56(0.2)	0.42(0.1)	0.33(0.1)	0.00(0.0)	0.00(0.0)	99.13	–	43	13	–	0.77	–	–
	ol(n = 2)	39.61(0.2)	0.01(0.0)	0.04(0.0)	16.72(0.1)	0.23(0.1)	45.1(0.2)	0.52(0.0)	0.00(0.0)	0.00(0.0)	0.00(0.0)	0.00(0.0)	102.23	83	–	–	–	–	–	–
6-1	gl(n = 5)	47.61(0.1)	0.67(0.1)	12.57(0.2)	9.38(0.2)	0.18(0.1)	8.42(0.1)	12.3(0.2)	2.1(0.1)	2.16(0.1)	0.46(0.1)	0.00(0.0)	95.85	–	–	–	–	0.62	–	0.98
6-2	gl(n = 5)	47.89(0.3)	0.77(0.1)	12.76(0.2)	9.55(0.1)	0.2(0.1)	8.19(0.1)	12.37(0.2)	2.15(0.1)	2.16(0.1)	0.47(0.0)	0.00(0.0)	96.52	–	–	–	–	0.60	–	0.97
6-3	gl(n = 5)	47.74(0.2)	0.71(0.0)	13.15(0.2)	9.75(0.3)	0.16(0.0)	7.73(0.4)	12.36(0.3)	2.27(0.1)	2.24(0.0)	0.48(0.1)	0.00(0.0)	96.57	–	–	–	–	0.59	–	0.94
	cpx(n = 4)	52.69(0.1)	0.42(0.1)	3.89(0.2)	4.74(0.1)	0.25(0.0)	16.19(0.0)	21.19(0.0)	0.63(0.1)	0.00(0.0)	0.00(0.0)	0.00(0.0)	100	–	48	7	–	0.86	–	–
	ol(n = 3)	41.1(0.2)	0.00(0.0)	0.00(0.0)	9.67(0.1)	0.21(0.0)	47.78(0.2)	0.59(0.0)	0.63(0.0)	0.01(0.0)	0.02(0.0)	0.00(0.0)	100	90	–	–	–	–	–	–
6-4	gl(n = 3)	49.11(0.1)	0.84(0.1)	14.03(0.4)	9.7(0.1)	0.17(0.1)	7.18(0.0)	11.71(0.1)	2.47(0.1)	2.37(0.1)	0.48(0.1)	0.00(0.0)	98.05	–	–	–	–	0.57	–	0.83
	cpx(n = 4)	51.52(0.6)	0.41(0.2)	5.57(0.5)	6.00(0.7)	0.18(0.1)	15.22(0.7)	20.37(0.4)	0.67(0.0)	0.05(0.1)	0.00(0.0)	0.00(0.0)	100	–	46	10	–	–	–	–
	ol(n = 3)	41.31(0.4)	0.03(0.0)	0.04(0.0)	11.27(0.3)	0.27(0.1)	46.00(0.3)	0.57(0.1)	0.77(0.0)	0.02(0.0)	0.00(0.0)	0.00(0.0)	100.28	88	–	–	–	–	–	–

Compositions of experimental glasses and minerals analyzed at EPMA. SOM-1, starting glass; other abbreviations as in Table 3. CaO/Al_2O_3 is calculated for the glass phase. In brackets standard deviation with n = number of analyses.

+0.5 and +1 yield Fo ~ 90 (charge #6-3, Table 2) and olivines with Fo < 85 all come from charges with ΔNNO < +1 and proportions of crystals between 21 and 54%.

Plagioclase was satisfactorily analyzed only in charge #5-5 (An_{67}, Table 3).

4.6. Experimental glass compositions

Upon progressive crystallization, experimental glasses shift from Som-1 towards more evolved compositions. Taking alternatively MgO or CaO/Al_2O_3 as a differentiation index, SiO_2, Al_2O_3, Na_2O, K_2O and P_2O_5 increase with differentiation whereas CaO and MgO decrease, the latter from 8.8 to 3.2 wt.% (Tables 3–4). FeO_{tot} and TiO_2 show little variations. In the most evolved glasses, SiO_2 contents reach ~55 wt.%, Al_2O_3 ~ 18 wt.% and K_2O ~ 5.5 wt.%, in the range of latitic whole-rock compositions at Vulcano (De Astis et al., 1997), and CaO/Al_2O_3 drops from ~1 to 0.36 (Tables 3–4). Glass in charge #2-3 (L + Cpx phase assemblage) plots in the range of glasses in L + Cpx + Ol charges, the latter covering most of the glass chemical range, from 8.2 to 3.5 wt.% MgO. Glasses in L + Cpx + Ol + Plag charges generally plot at the evolved ends (highest SiO_2, Al_2O_3 and K_2O) of compositional trends.

Cotectic (Cpx + Ol co-saturated) glasses at 1150 °C have CaO decreasing with the MgO concentration (Fig. 8). At a given MgO, the CaO concentration systematically increases with decreasing pressure from 154, 88 to 44 MPa, in agreement with previous results (Pichavant et al., 2009). The Som-1 composition plots on extensions of the 44 and 88 MPa cotectics, suggesting that, in this range of pressures and for a temperature of 1150 °C, clinopyroxene and olivine could appear together on the Som-1 liquidus. Therefore, the clinopyroxene and olivine saturation curves (Fig. 7) have been drawn closer to each other with decreasing pressure. Relative to the extension of the 154 MPa cotectic, Som-1 plots in the Cpx field, consistent with the determined phase relations (clinopyroxene slightly earlier than olivine at 150 MPa, Fig. 6).

5. Magmatic evolution at Vulcano

Below, experimental results on Som-1 are used to constrain the magmatic evolution at Vulcano. To do so, an inverse approach will be applied, i.e., the Vulcano differentiation sequence will be examined "uphill", beginning with relatively evolved compositions to progressively constrain the characteristics of primitive, possibly primary, melts, and discuss their origin as well as the nature of the early differentiation processes.

5.1. Magma differentiation

First, experimental glasses are compared with the La Sommata MI compositions (Fig. 8). The 44 MPa cotectic experimental glasses and the glass inclusions in clinopyroxene overlap. This suggests that small degrees of crystallization of a Som-1 type melt at low pressures can generate liquid compositions similar to MI trapped in clinopyroxene. Thus, MI in clinopyroxene simply represent melts generated during the initial stages of crystallization-differentiation of Som-1 like shoshonitic basaltic liquids. It is worth emphasizing here that MI in clinopyroxene have a less marked ultra-calcic character (lower CaO and CaO/Al_2O_3) than MI in olivine (Figs. 2, 8). The latter have CaO and CaO/Al_2O_3 markedly higher than all experimental glasses and they follow a slightly negative trend in the CaO vs. MgO diagram (Fig. 8) that contrasts with the positive trend for cotectic glasses and clinopyroxene MI. In other diagrams (e.g., CaO/Al_2O_3 vs. SiO_2, Al_2O_3 or K_2O, not shown), MI in olivine plot opposite to experimental differentiation trends, extending to SiO_2, Al_2O_3 and K_2O lower than in Som-1. Clearly, glass inclusions in olivine differ from melts generated from the crystallization of Som-1 type melts.

Second, experimental glasses are compared with whole-rock compositions erupted at Vulcano. To do so, products from the Caldera del Piano (De Astis et al., 1997) and from the opening phases of the Caldera della Fossa (Gioncada et al., 1998), both broadly contemporaneous with the La Sommata eruption, have been selected. In the CaO/Al_2O_3 vs. MgO plot (Fig. 9), as well as in other diagrams (not shown), experimental glasses and whole-rock compositions closely overlap. This indicates that progressive crystallization of Som-1 type magmas can generate differentiated melts (Fig. 9), in the range of latitic whole-rocks on Vulcano (i.e., >56 wt.% SiO_2, < 2 wt.% MgO, De Astis et al., 1997). We conclude that primitive melts such as the La Sommata basalt can be parental both to melts trapped in clinopyroxene and to the primitive part (i.e., 48–55 wt.% SiO_2) of the shoshonitic sequence at Vulcano.

5.2. Composition of the primitive end-member magma

Conclusions above about magma differentiation leave open the questions of (1) the composition of the primitive end-member magma at Vulcano, (2) the mechanism of generation of melts such as the olivine MI and (3) the mutual relationships between MI in olivine,

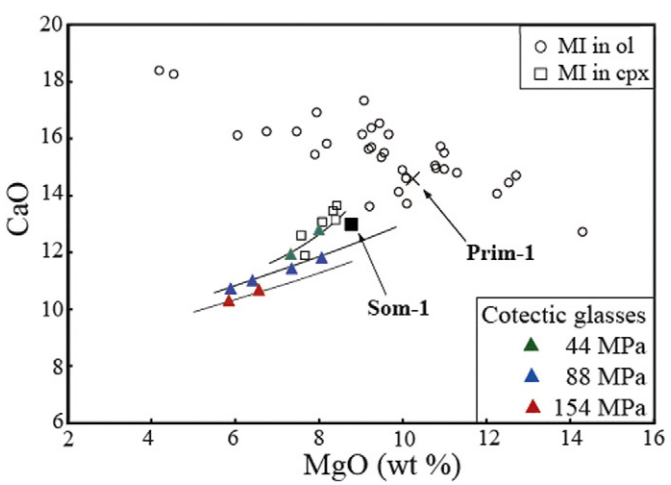


Fig. 8. CaO vs. MgO plot showing compositions of cotectic (Cpx + Ol co-saturated) experimental glasses at 1150 °C and of glass inclusions in the La Sommata basalt. Data for the experimental glasses (Table 4, normalized to 100 wt.%) are distinguished by pressure (44, 88, 154 MPa, Table 2). Melt inclusion data as in Fig. 1. The compositions of the La Sommata basalt (Som-1) and of the theoretical primitive end-member magma (Prim-1) are shown (see Table 1).

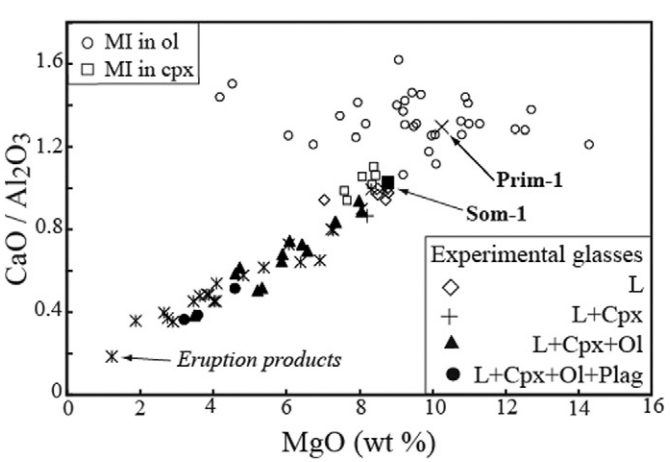


Fig. 9. CaO/Al_2O_3 vs. MgO plot showing compositions of experimental glasses from this study, of melt inclusions in the La Sommata basalt and of selected eruption products from Vulcano (see text). Melt inclusion data as in Fig. 1. For the experimental glasses, the data (Tables 3–4, normalized to 100 wt.%) are distinguished by phase assemblage. Whole-rock compositions from De Astis et al. (1997) and Gioncada et al. (1998). The compositions of the La Sommata basalt (Som-1) and of the theoretical primitive end-member magma (Prim-1) are shown (see Table 1).

on the one hand, and MI in clinopyroxene, on the other hand. These are important issues since MI in La Sommata olivine are being used as reference samples for a variety of purposes (Schiano et al., 2006; Mercier et al., 2010) and, therefore, their compositional significance needs to be established.

The theoretical composition of the primitive end-member basaltic melt at Vulcano has been estimated starting from the suggestion (Gioncada et al., 1998) that the La Sommata basalt represents a mixture between a primitive and a shoshonitic magma in a 80:20 proportion. Accordingly, 20% shoshonite has been subtracted from the Som-1 composition (Table 1) to generate the composition of the primitive end-member magma. To do so, different shoshonitic end-members were tested (De Astis et al., 1997; Gioncada et al., 1998) and different end-member magma compositions calculated. However, the results are not strongly dependent on the particular choice of the shoshonitic end-member and a representative composition of the primitive end-member basaltic melt (Prim-1) is given in Table 1. It has 47.7 wt.% SiO_2, 1.90 wt.% K_2O and 10.25 wt.% MgO which would classify it as a shoshonitic basalt. Compared to Som-1, Prim-1 is shifted towards lower SiO_2, Al_2O_3 and K_2O, and higher CaO and MgO. $Fo_{90.8}$ olivine is calculated to be at equilibrium with Prim-1 (calculations performed at NNO + 1 and with $K_d^{Fe-Mg}{}_{ol-liq} = 0.25$, see above), in the range of the most Fo-rich crystals in the La Sommata basalt. Prim-1 has a very elevated CaO/Al_2O_3 (1.30), is strongly *ne*-normative (10% *ne*) and plots in the middle of the olivine MI group (Figs. 8, 9). We conclude that the theoretical composition of the primitive end-member is virtually identical to the average of MI in La Sommata olivines. This strongly suggests that those MI are representative of end-member primitive basaltic liquids present at Vulcano, in particular during the pre-Lentia caldera activity. MI in La Sommata olivine thus represent remnants of those primitive parental melts which underwent mixing with more differentiated products to eventually produce Som-1 type magmas. Upon subsequent differentiation, compositions such as the clinopyroxene MI and the least fractionated terms of the shoshonitic series were generated (Fig. 10).

6. Origin of the ultra-calcic arc melt signature

We stress that the end-member primitive basaltic melt defined above has a marked ultra-calcic affinity (SiO_2 < 48 wt.%, $Na_2O + K_2O > 3$ wt.%, MgO = 10.25 wt.%, $CaO/Al_2O_3 \gg 1$, 10% normative *ne*, Schiano et al., 2000). Therefore, the origin of such primitive compositions needs to be clarified. Below, we combine our experimental results on Som-1 with evidence from Aeolian arc volcanoes to propose a revised interpretation for the origin of ultra-calcic arc melt compositions.

6.1. Liquidus phase equilibria of the La Sommata basalt Som-1

In our experiments on hydrous Som-1 melt, clinopyroxene, olivine and plagioclase occur as the major crystallizing phases. Three experimental assemblages have been found: L + Cpx, L + Cpx + Ol and L + Cpx + Ol + Plag. Except above the liquidus, clinopyroxene-free assemblages are absent. Note that Fe-oxide should be added to the three assemblages above, although its presence has not been confirmed in all charges. Orthopyroxene (Opx) has not been encountered, despite experiments being performed well below the liquidus and residual melts reaching SiO_2 contents ~55 wt.% (compare with other phase equilibrium studies on primitive basalts, e.g., Pichavant and Macdonald, 2007).

One characteristic feature of experimental phase equilibria for Som-1 is that clinopyroxene is the liquidus phase at 150 MPa, an unexpectedly low pressure range on the basis of previous experimental studies on basalts (e.g. Gust and Perfit, 1987; Falloon et al., 1999; Pichavant et al., 2002). Clinopyroxene (and also orthopyroxene for primary melts from a lherzolite source) is expected to saturate at relatively high pressures on the liquidus of primary basalts. Olivine would saturate at lower pressures and, for primary basaltic melts, multiple saturation points are usually found in the range 1–1.2 GPa, or higher if the system is hydrous (e.g. Pichavant et al., 2002). In the case of Som-1, co-saturation of olivine and clinopyroxene on the liquidus occurs at very low pressures. At 150 MPa, Cpx and Ol are very close to appear together on the liquidus, only one charge demonstrating that Cpx crystallizes earlier than Ol (Fig. 6). At 1150 °C, Ol would join Cpx on the hydrous Som-1 liquidus at a pressure lower than 150 MPa, most probably between 44 and 88 MPa since the Som-1 bulk composition lies in between the extension of the 44 and 88 MPa cotectics (Figs. 7, 8). Such a very low pressure range for Ol and Cpx co-saturation, and the total absence of Opx on the liquidus, are very unusual features for a relatively primitive basalt.

To check whether our experimental results are influenced by the particular choice of Som-1 as starting material, MELTS calculations have been performed on the Prim-1 composition. Near liquidus phase equilibria were computed (Ghiorso and Sack, 1995) on Prim-1 and also for consistency on Som-1. The calculations were performed for different pressures, constant $H_2O_{melt} = 3.5$ wt.% and a fO_2 set at NNO + 1. For Som-1 at 150 MPa, MELTS finds Ol to appear first on the liquidus at 1178 °C; Cpx comes in second at 1145 °C. For Prim-1, Ol is also the liquidus phase, crystallizing at 1194 °C and Cpx at 1160 °C so that Cpx

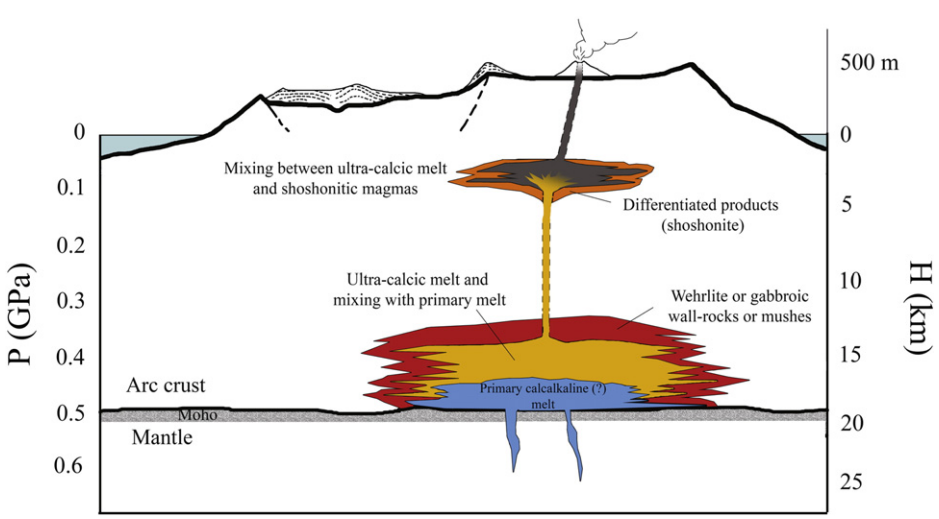


Fig. 10. Schematic representation of the Vulcano plumbing system (after De Astis et al., 2013) showing the mantle–crust boundary and the lower and upper magma accumulation zones. Interaction between a primary calk-alkaline (?) melt and wehrlite or gabbroic wall-rock lithologies in the deep part of the plumbing system generates ultra-calcic melts. The ultra-calcic melts then ascend to the upper accumulation zone where it mixes with differentiated magmas (shoshonite-latite) to produce the La Sommata basalt. See text for details.

appears either 33 (Som-1) or 34 °C (Prim-1) below the 150 MPa liquidus. Upon increasing pressure, Cpx joins Ol on the liquidus, at either 520 MPa (Som-1) or 560 MPa (Prim-1). Therefore, although MELTS fails to reproduce our experimental results, pressures ≪ 1 GPa are confirmed for Cpx + Ol co-saturation, both for Prim-1 and Som-1. Most importantly, MELTS calculations do not support a major difference in phase relations between Som-1 and Prim-1, which indicates that our experimental results are representative and applicable to discuss the origin of primitive ultra-calcic magmas at Vulcano.

6.2. Liquidus phase equilibria of ultra-calcic arc melts: comparison between synthetic and natural compositions

Médard et al. (2004) carried out near-liquidus experiments on a synthetic composition (CaNe) representative of ultra-calcic arc compositions. Cpx was found as the liquidus phase at 500 and 700 MPa, and Ol as the liquidus phase at 0.1 MPa. A pressure of ~200 MPa was determined for Cpx + Ol co-saturation on the CaNe liquidus at a temperature of 1220 °C. The third phase to appear in the crystallization sequence was plagioclase and orthopyroxene was not encountered (Médard et al., 2004). Therefore, phase relations determined in this study for the La Sommata basalt are identical in critical aspects to those obtained on the synthetic CaNe ultra-calcic composition (Médard et al., 2004). Liquidus temperatures higher than in this work were found in Médard et al. (2004), a consequence of the use of nominally anhydrous compositions in the latter study. We conclude that experiments on both natural (Som-1) and synthetic (CaNe) arc ultra-calcic compositions yield phase equilibrium results that are essentially identical.

6.3. Origin of ultra-calcic arc melts

Ultra-calcic arc melts have been initially interpreted as primary compositions generated by melting of specific mantle sources. Experimental results have provided constraints on the nature of possible source rocks (e.g., Kogiso and Hirschmann, 2001; Médard et al., 2004, 2006; Sorbadere et al., 2013). For their synthetic CaNe ultra-calcic arc composition, Médard et al. (2004) found either Cpx or Ol crystallizing on the liquidus, consistent with an origin by partial melting of a source rock leaving either clinopyroxene or olivine as residual phases. They noted the very low pressure (~200 MPa) of Cpx + Ol co-saturation on the CaNe liquidus. Such an abnormally low pressure range was explained by olivine fractionation, the CaNe composition investigated being olivine-depleted, yet a maximum pressure of 1 GPa was inferred for CaNe to be at equilibrium with a wehrlitic residual assemblage (Médard et al., 2004). Therefore, it was concluded that ultra-calcic melts must be generated in the arc crust (Médard et al., 2004). This interpretation is clearly strengthened by our experimental results. Co-saturation of Cpx + Ol on the liquidus of Som-1 occurs at very low pressures, being located between 44 and 88 MPa at 1150 °C (see above). Although Som-1 is not exactly representative of the end-member ultra-calcic melt at Vulcano (because of mixing with the shoshonitic magma, see above), MELTS calculations for Som-1 and Prim-1 yield Cpx + Ol co-saturation pressures that are within 50 MPa of each other. Therefore, an end-member primitive ultra-calcic arc melt such as Prim-1 presumably would be co-saturated with a wehrlite mineral assemblage at pressures not much higher than Som-1, i.e., ≪1 GPa. The inverse dependence of the CaO content of cotectic melts with pressure (Fig. 8; see also Pichavant et al., 2009) provides a simple yet powerful indication for ultra-calcic melts being generated at very low pressures: for a composition such as Som-1 to be cosaturated with a wehrlitic phase assemblage, pressures ≤100 MPa are necessary.

If ultra-calcic arc melts indeed represent primary compositions, then both the results of Médard et al. (2004) and of this study require another mineral phase to be involved in the partial melting process. Amphibole was proposed by Médard et al. (2004) to be an ideal candidate because it would impart to the partial melt the *ne*-normative, alkali-rich, character typical of the ultra-calcic signature. The interpretation originally proposed for the origin of ultra-calcic arc melts involves sequential melting of an amphibole wehrlite source (Médard et al., 2006; Sorbadere et al., 2013). Amphibole would be the first phase to be consumed during the melting process, leaving a refractory wehrlitic residual mineralogy, consistent with the liquidus phase equilibria determined for both CaNe and Som-1, and yielding a melt whose composition is controlled by the proportion of amphibole in the source and the peak melting temperature (Kogiso and Hirschmann, 2001).

However, ultra-calcic compositions might also represent derivative (i.e., non-primary) melts. Danyushevsky et al. (2004) have shown that ultra-calcic glass inclusion compositions can originate during complex localized dissolution-reaction-mixing processes within magmatic plumbing systems. This type of process occurs at the margins of primitive magma bodies, where newly injected, hotter, primitive magma comes into contact with previously solidified, cooler, wall-rocks, either cumulates or crystal mushes. Dissolution of mineral phases from the mush, mixing of reaction products with the primitive melt, and coupled crystallization of olivine from the primitive magma, may lead to the trapping of the generated ultra-calcic melts as MI.

One way to distinguish between the two types of models (primary vs. non-primary) is to constrain the pressure range to generate compositions such as Som-1 and Prim-1. From our experimental results, Som-1 can be generated at equilibrium with a wehrlite assemblage at ≤100 MPa and Prim-1 at a pressure slightly higher. We note, however, that the data also make it possible that Som-1 (and Prim-1) are generated at equilibrium with a clinopyroxenite assemblage which would imply higher pressures. Nevertheless, in this case, clinopyroxene would be much earlier than olivine in the crystallization sequence, which is observed neither in the experiments (Figs. 6, 7) nor in the rocks (compositions of the most primitive Ol and Cpx are broadly in equilibrium and textural evidence suggests cotectic crystallization). Therefore, the only possibility remaining is that the ultra-calcic melt is generated at equilibrium with a cotectic (wehrlite) assemblage, implying that the pressure of crystallization of the cotectic assemblage (for appropriate values of temperature and melt H_2O concentration) gives the pressure of melt generation. Considering the pressure range implied by our results (for Som-1 ≤ 100 MPa at 1150 °C and 2.5 wt.% H_2O, Fig. 7), it seems difficult to consider ultra-calcic arc compositions as primary melts generated at mantle depths. Rather, we propose that these specific compositions record the interaction between primitive, presumably peridotite-derived melts and clinopyroxene-rich wall-rocks, cumulates or mushes, that are present in the arc crust, most probably as products of the crystallization of older magma batches. A similar two-component model was proposed by Sorbadere et al. (2013) who showed that ultra-calcic arc melts are products of mixing between partial melts from peridotite and from amphibole-bearing clinopyroxenite.

6.4. Evidence from the Aeolian arc

Both Vulcano and Stromboli offer the opportunity to apply and refine the general model above. Concerning Vulcano, our experimental results are combined with data on La Sommata MI and results of MELTS calculations to infer the pressure of crystallization of the cotectic clinopyroxene + olivine assemblage in Prim-1 which, from above, determines the depth of the melt-wall-rock interaction process that generates the ultra-calcic liquids.

Gioncada et al. (1998) reported a range of H_2O concentrations of 1.8–3.8% in La Sommata olivine MI and determined MI homogenization temperatures (T_h). The recent results of Mercier et al. (2010) imply higher H_2O_{melt}, 3.8–4.5 wt.%. Gioncada et al. (1998) reported systematically higher T_h for olivine than for clinopyroxene MI. However, the high T_h (>1250 °C) found for MI in olivine most probably reflect loss of volatiles during heating (Gioncada et al., 1998) since clinopyroxene and olivine crystallize very close to each other in Som-1 (Figs. 4, 6, 7). The

gaussian T_h distribution (centered at 1160 °C) for MI in clinopyroxene suggests that those MI record temperatures the closer to real trapping values (Gioncada et al., 1998).

Conditions of crystallization of the cotectic assemblage can be constrained from experimental phase equilibria. It is readily apparent from the isothermal section (Fig. 7) that co-precipitation of clinopyroxene + olivine at 1150 °C requires a pressure of 150 MPa minimum for H_2O_{melt} = 2.7 wt.%, the cosaturation pressure increasing with H_2O_{melt}. At 150 MPa, a temperature beyond 1150 °C would be necessary for the co-precipitation of clinopyroxene + olivine if H_2O_{melt} is <3 wt.% (i.e., 1180–1200 °C for 2.5 wt.% H_2O, Fig. 6). Assuming 1160 °C (the median of T_h for clinopyroxene MI, Gioncada et al., 1998) as the temperature of co-precipitation of clinopyroxene and olivine and taking a range of H_2O_{melt} between 3.5 and 4.0 wt.% (Mercier et al., 2010), pressures >150 MPa are required for the crystallization of the cotectic assemblage in Prim-1. Using a P-T-H_2O_{melt} grid constructed from our experimental data (see Di Carlo et al., 2006; their Figure 11) and incorporating temperature corrections from our MELTS calculations to account for the compositional difference between Som-1 and Prim-1, a pressure range between 250 and 350 MPa is inferred for Cpx + Ol co-saturation in Prim-1. In the context of the Aeolian Arc, this corresponds to middle crustal pressures (i.e., to 9–13 km with a crustal density of 2700 kg m^{-3}) since the Moho beneath Vulcano is located at ~20 km depth (De Astis et al., 2013).

The model proposed for La Sommata involves interaction between a primary melt generated in a presumably peridotitic mantle wedge and wehrlitic (or gabbroic) rocks residing in the middle to lower parts of the Aeolian arc crust. Evidence for wehrlite is missing at Vulcano although wehrlitic and clinopyroxenitic enclaves are known on several other Aeolian islands (Peccerillo et al., 2004; Laiolo and Cigolini, 2006). Gabbroic bodies occur both at Vulcano (Faraone et al., 1986) and on other islands (Salvioli-Mariani et al., 2002; Mattioli et al., 2003; Laiolo and Cigolini, 2006). The melt-wall-rock interaction process would produce a three component mixture between a primary (unreacted) melt (not observed at Vulcano), an ultra-calcic melt locally present within the melt-mush reaction zone and an assemblage of newly formed clinopyroxene and olivine crystals. From the pressure range estimated above, the interaction process would take place in the lower part of the plumbing system, most probably in the lower magma accumulation zone, located at 190–350 MPa (Clocchiatti et al., 1994), 250–500 MPa (Zanon et al., 2003) or 300–500 MPa (De Astis et al., 2013) beneath Vulcano. Previous work has suggested that this zone is the main site for magma recharge, differentiation, AFC and mixing (Zanon et al., 2003; De Astis et al., 2013). Prim-1 type magmas, following their generation in this deep reservoir, may later ascend and mix with more differentiated products to generate magmas represented by the La Sommata basalt (Fig. 10).

This general model bears strong similarities with the deep magmatic evolution at Stromboli. The golden pumice PST-9 has clinopyroxene preceding olivine in the crystallization sequence at 400 MPa, and is cosaturated with Cpx + Ol at ~150 MPa (1100 °C, H_2O_{melt} = 3.5 wt.%, Di Carlo et al., 2006), in a similar pressure range as other ultra-calcic compositions such as Som-1 and CaNe. Barometric estimates from H_2O–CO_2 systematics and experimental results demonstrate that the ultra-calcic MI in Stromboli olivine (Fig. 2) were trapped at crustal pressures (between 150 and 250 MPa, Pichavant et al., 2009, 2011; Métrich et al., 2010). Those MI plot in the Cpx primary field yet they are found trapped in olivine crystals implying that they represent local melts (Pichavant et al., 2009). Assimilation of dunite and wehrlite lithologies is necessary to explain the trace element geochemistry of golden pumices (Schiavi et al., 2010). Therefore, in an analogous way to Prim-1 at Vulcano, golden pumice magmas at Stromboli are the result of the interaction between primitive, mantle-derived, melts and clinopyroxene-rich lithologies in the plumbing system (Pichavant et al., 2009, 2011).

7. Summary and conclusions

(1) Two main groups of primitive compositions occur in the Aeolian arc: calc-alkaline (Alicudi basalts, possibly some seamount basalts) and ultra-calcic (Vulcano basalts, Vulcano and Stromboli MI). The ultra-calcic signature may be a common feature in the Aeolian arc.

(2) On Vulcano, the La Sommata basalt is a reference primitive *ne*-normative arc basalt with a strong ultra-calcic affinity. Although it does not correspond exactly to an end-member primitive liquid, the La Sommata basalt is a natural proxy of an ultra-calcic arc melt and, as such, it offers the opportunity to document the phase relations of a natural ultra-calcic arc composition.

(3) Experimental phase equilibria for Som-1 (determined between 44 and 154 MPa, for 0.7–3.5 wt.% H_2O and fO_2 between NNO + 0.2 and +1.9) show clinopyroxene slightly preceding olivine at 150 MPa and olivine joining clinopyroxene on the liquidus between 44 and 88 MPa. Plagioclase is the third phase in the crystallization sequence. Orthopyroxene is lacking.

(4) Cotectic experimental glasses and natural glass inclusions in clinopyroxene overlap. Upon progressive crystallization, experimental glasses shift from Som-1 towards more evolved compositions similar to latitic whole-rocks erupted at Vulcano. Melts such as the La Sommata basalt can be parental both to melts trapped in clinopyroxene and to the least fractionated part (i.e., 48–55 wt.% SiO_2) of the shoshonitic sequence at Vulcano, erupted in the same period.

(5) The calculated composition of the end-member primitive melt is virtually identical to the average of MI in La Sommata olivines. Therefore, MI in olivine are representative of end-member primitive basaltic liquids at Vulcano. Such primitive melts mixed with more differentiated products to eventually produce the La Sommata basalt.

(6) The experimental results on the La Sommata basalt are identical in critical aspects to those obtained previously on a synthetic ultra-calcic arc composition. Phase relations for the end-member primitive melt, calculated with MELTS, are not significantly different from those determined on the La Sommata basalt. All experimental results suggest that generation of primitive ultra-calcic melts leaves a clinopyroxene-rich residual source, either wehrlite at low pressures or clinopyroxenite at higher pressures.

(7) A wehrlitic residual source is implied by the mineralogical and petrographical characteristics of the La Sommata products. Thus, ultra-calcic arc compositions at Vulcano are generated at crustal pressures. They represent non-primary melts produced by the interaction between primary, presumably peridotite-derived melts, and clinopyroxene-rich wall-rocks in the Aeolian arc crust.

(8) The La Sommata basalt and MI record a process of interaction between a primary melt generated in the mantle wedge (not observed at Vulcano) and wehrlitic or gabbroic rocks present in the lower part of the plumbing system. The interaction process is inferred to take place between 250 and 350 MPa, most probably in the lower magma accumulation zone beneath Vulcano.

(9) The model proposed for Vulcano has close similarities with the deep magmatic evolution at Stromboli. Primitive ultra-calcic magmas in the Aeolian arc are generated at crustal instead of mantellic conditions.

Acknowledgements

This work is based on the PhD thesis of the first author which was supported both by the University of Palermo and the University of Orléans. Funding by an FFR grant of the University of Palermo to SGR and by an ESF grant (in the framework of the MeMoVolc program) to GL is acknowledged. The final version has benefited from the constructive comments of an anonymous reviewer and of the Editor.

References

Arrighi, S., Tanguy, J., Rosi, M., 2006. Eruptions of the last 2200 years at Vulcano and Vulcanello (Aeolian Islands, Italy) dated by high-accuracy paleomagnetism. Phys. Earth Planet. Inter. 159, 225–233.

Ballhaus, C., Berry, C.F., Green, D.H., 1991. High pressure experimental calibration of the olivine-orthopyroxene-spinel oxygen geobarometer: implications for the oxidation state of the upper mantle. Contrib. Mineral. Petrol. 108, 82–92.

Barclay, J., Carmichael, I.S.E., 2004. A hornblende basalt from western Mexico: water-saturated phase relations constrain a pressure–temperature window of eruptibility. J. Petrol. 45, 485–506.

Beccaluva, L., Gabbianelli, G., Lucchini, F., Rossi, P.L., Savelli, C., 1985. Petrology and K/Ar ages of volcanics dredged from the Eolian seamounts: implications for geodynamic evolution of the southern Tyrrhenian basin. Earth Planet. Sci. Lett. 74, 187–208.

Bertagnini, A., Métrich, N., Landi, P., Rosi, M., 2003. Stromboli volcano (Aeolian Archipelago, Italy): an open window on the deep-feeding system of a steady state basaltic volcano. J. Geophys. Res. 108 (B7). http://dx.doi.org/10.1029/ 2002JB002146.

Burnham, C.W., 1979. The importance of volatile constituents. In: Yoder Jr., H.S. (Ed.), The Evolution of Igneous Rocks. Princeton, NJ, pp. 439–482.

Chen, Y., Provost, A., Schiano, P., Cluzel, N., 2013. Magma ascent rate and initial water concentration inferred from diffusive water loss from olivine-hosted melt inclusions. Contrib. Mineral. Petrol. 165, 525–541.

Clocchiatti, R., Del Moro, A., Gioncada, A., Joron, J.L., Mosbah, M., Pinarelli, L., Sbrana, A., 1994. Assessment of a shallow magmatic system: the 1888–90 eruption, Vulcano Island, Italy. Bull. Volcanol. 56, 466–486.

Danyushevsky, L.V., Leslie, R.A.J., Crawford, A.J., Durance, P., 2004. Melt inclusions in primitive olivine phenocrysts: the role of localized reaction processes in the origin of anomalous compositions. J. Petrol. 45, 2531–2553.

De Astis, G., La Volpe, L., Peccerillo, A., Civetta, L., 1997. Volcanological and petrological evolution of Vulcano island (Aeolian Arc, southern Tyrrhenian Sea). J. Geophys. Res. 102, 8021–8050.

De Astis, G., Lucchi, F., Dellino, P., La Volpe, L., Tranne, C.A., Frezzotti, M.L., Peccerillo, A., 2013. Geology, volcanic history and petrology of Vulcano (central Aeolian archipelago. In: Lucchi, F., Peccerillo, A., Keller, J., CA, T., Rossi, P.L. (Eds.), The Aeolian Islands Volcanoes. Geological Society of London Memoirs Vol. 37, pp. 281–349.

De Astis, G., Lucchi, F., Tranne, C.A., 2006. The Aeolian volcanic district: volcanism and magmatism. Acta Volcanol. 18, 79–104.

De Astis, G.F., Peccerillo, A., Kempton, P.D., La Volpe, L., Wu, T.W., 2000. Transition from calc-alkaline to potassium-rich magmatism in subduction environments: geochemical and Sr, Nd, Pb isotopic constraints from the Island of Vulcano (Aeolian Arc). Contrib. Mineral. Petrol. 139, 684–703.

Del Moro, A., Gioncada, A., Pinarelli, L., Sbrana, A., Joron, J.L., 1998. Sr, Nd, and Pb isotope evidence for open system evolution at Vulcano, Aeolian Arc, Italy. Lithos 43, 81–106.

Devine, J.D., Gardner, J.E., Brack, H.P., Layne, G.D., Rtherford, M.J., 1995. Comparison of microanalytical methods for estimating H_2O contents of silicic volcanic glasses. Am. Mineral. 80, 319–328.

Di Carlo, I., Pichavant, M., Rotolo, S.G., Scaillet, B., 2006. Experimental crystallization of a high-K arc basalt: the Golden Pumice, Stromboli volcano (Italy). J. Petrol. 47, 1317–1343.

Drummond, M.S., Defant, M.J., 1990. A model for trondhjemite-tonalite-dacite genesis and crustal growth via slab melting: archean to modern comparisons. J. Geophys. Res. 95, 21503–21521.

Falloon, T.J., Green, D.H., Jacques, A.L., Hawkins, J.W., 1999. Refractory magmas in back-arc basin settings — experimental constraints on the petrogenesis of a Lau Basin example. J. Petrol. 40, 255–277.

Faraone, D., Silvano, A., Verdiani, G., 1986. The monzogabbroic intrusion in the Island of Vulcano, Aeolian Archipelago, Italy. Bull. Volcanol. 48, 299–307.

Georgiev, S., Marchev, P., Heinrich, C.A., von Quadt, A., Peytcheva, I., Manetti, P., 2009. Origin of nepheline-normative high-K ankaramites and the evolution of eastern Srednogorie arc in SE Europe. J. Petrol. 50, 1899–1933.

Ghiorso, M., Sack, R., 1995. Chemical mass transfer in magmatic processes. IV. A revised and internally consistent thermodynamic model for the interpolation and extrapolation of liquid–solid equilibria in magmatic systems at elevated temperatures and pressures. Contrib. Mineral. Petrol. 119, 197–212.

Gioncada, A., Clocchiatti, R., Sbrana, A., Bottazzi, P., Massare, D., Ottolini, L., 1998. A study of melt inclusions at Vulcano (Aeolian Islands, Italy): insights on the primitive magmas and on the volcanic feedings system. Bull. Volcanol. 60, 286–306.

Green, D.H., Schmidt, M.W., Hibberson, W.O., 2004. Island-arc ankaramites: primitive melts from fluxed refractory lherzolitic mantle. J. Petrol. 45, 391–403.

Grove, T.L., Donnelly-Nolan, J.M., Housh, T., 1997. Magmatic processes that generated the rhyolite of Glass Mountain, Medicine Lake volcano, N. California. Contrib. Mineral. Petrol. 127, 205–223.

Gust, D.A., Perfit, M.R., 1987. Phase relations of a high-Mg basalt from the Aleutian island arc: implications for primary island arc basalts and high-Al basalts. Contrib. Mineral. Petrol. 97, 7–18.

Kamenetsky, V., Clocchiatti, R., 1996. Primitive magmatism of Mt. Etna: insights from mineralogy and melt inclusions. Earth Planet. Sci. Lett. 142, 553–572.

Keller, J., 1974. Petrology of some volcanic rock series of the Aeolian Arc, southern Tyrrhenian Sea: calc-alkaline and shoshonitic associations. Contrib. Mineral. Petrol. 46, 29–47.

Kogiso, T., Hirschmann, M.M., 2001. Experimental study of clinopyroxenite partial melting and the origin of ultra-calcic melt inclusions. Contrib. Mineral. Petrol. 142, 347–360.

Kress, V.C., Carmichael, S.E., 1991. The compressibility of silicate liquids containing Fe_2O_3 and the effect of composition, temperature, oxygen fugacity and pressure on their redox state. Contrib. Mineral. Petrol. 108, 82–92.

Laiolo, M., Cigolini, C., 2006. Mafic and ultramafic xenoliths in San Bartolo lava field: new insights on the ascent and storage of Stromboli magmas. Bull. Volcanol. 68, 653–670.

Marchev, P., Georgiev, S., Zajacz, Z., Manetti, P., Raicheva, R., von Quadt, A., Tommasini, S., 2009. High-K ankaramitic melt inclusions and lavas in the Upper Cretaceous Eastern Srednogorie continental arc, Bulgaria: implications for the genesis of arc shoshonites. Lithos 113, 228–245.

Mattioli, M., Serri, G., Salvioli-Mariani, E., Renzulli, A., Holm, P.M., Santi, P., Venturelli, G., 2003. Sub-volcanic infiltration and syneruptive quenching of liquids in cumulate wall-rocks: the example of the gabbroic nodules of Stromboli (Aeolian islands, Italy). Mineral. Petrol. 78, 201–230.

Médard, E., Schmidt, M.W., Schiano, P., 2004. Liquidus surface of ultra-calcic primitive melts: formation conditions and sources. Contrib. Mineral. Petrol. 148, 201–215.

Médard, E., Schmidt, M.W., Schiano, P., Ottolini, L., 2006. Melting of amphibole-bearing wehrlites: an experimental study on the origin of ultra-calcic nepheline-normative melts. J. Petrol. 47, 481–504.

Mercier, M., Di Muro, A., Métrich, N., Giordano, D., Belhadj, O., Mandeville, C.W., 2010. Spectroscopic analysis (FTIR, RAMAN) of water in mafic and intermediate glasses and glass inclusions. Geochim. Cosmochim. Acta 74, 5641–5656.

Métrich, N., Clocchiatti, R., 1996. Sulfur abundance and its speciation in oxidized alkaline melts. Geochim. Cosmochim. Acta 60, 4151–4160.

Métrich, N., Bertagnini, A., Di Muro, A., 2010. Conditions of magma storage, degassing and ascent at Stromboli: new insights into the volcanic plumbing system with inferences on the eruptive dynamics. J. Petrol. 51, 603–626.

Muncill, G.E., Lasaga, A.C., 1987. Crystal-growth kinetics of plagioclase in igneous systems: one-atmosphere experiments and application of a simplified growth model. Am. Mineral. 72, 299–311.

Peccerillo, A., 2005. Plio-Quaternary volcanism in Italy. Petrology, geochemistry, geodynamics. Springer, Berlin Heidelberg New York, p. 365.

Peccerillo, A., Dallai, L., Frezzotti, M.L., Kempton, P.D., 2004. Sr-Nd-Pb-O isotopic evidence for decreasing crustal contamination with ongoing magma evolution at Alicudi volcano (Aeolian Arc, Italy): implication for style of magma-crust interaction and mantle source compositions. Lithos 78, 217–233.

Peccerillo, A., De Astis, G., Faraone, D., Forni, F., Frezzotti, M.L., 2013. Compositional variations of magmas in the Aeolian arc: implications for petrogenesis and geodynamics. In: Lucchi F, Peccerillo A, Keller J, Tranne CA, Rossi PL (Eds), The Aeolian Islands Volcanoes. Geol. Soc. Lond. Mem. 37, 491–510.

Pichavant, M., Macdonald, R., 2007. Crystallization of primitive basaltic magmas at crustal pressures and genesis of the calc-alkaline igneous suite: experimental evidence from St Vincent, Lesser Antilles arc. Contrib. Mineral. Petrol. 154, 535–558.

Pichavant, M., Di Carlo, I., Le Gac, Y., Rotolo, S.G., Scaillet, B., 2009. Experimental constraints on the deep magma feeding system at Stromboli Volcano, Italy. J. Petrol. 50, 601–624.

Pichavant, M., Mysen, B.O., Macdonald, R., 2002. Source and H_2O content of high-MgO magmas in island arc settings: an experimental study of a primitive calc-alkaline basalt from St. Vincent, Lesser Antilles arc. Geochim. Cosmochim. Acta 66, 2193–2209.

Pichavant, M., Pompilio, M., D'Oriano, C., Di Carlo, I., 2011. Petrography, mineralogy and geochemistry of a primitive pumice from Stromboli: implications for the deep feeding system. Eur. J. Mineral. 23, 499–517.

Piochi, M., De Astis, G., Petrelli, M., Ventura, G., Sulpizio, R., Zanetti, A., 2009. Constraining the recent plumbing system of Vulcano (Aeolian Arc, Italy) by textural, petrological, and fractal analysis: the 1739 A.D. Pietre Cotte lava flow. Geochem. Geophys. Geosyst. 10, Q01009. http://dx.doi.org/10.1029/2008GC002176.

Robie, R.A., Hemingway, B.S., Fisher, J.R., 1979. Thermodynamic properties of minerals and related substances at 298.15 K and 1 bar (10^5 pascals) pressure and at higher temperatures. U.S. Geol. Surv. Bull. 1452, 456.

Rose-Koga, E.F., Koga, K.T., Schiano, P., Le Voyer, M., Shimizu, N., Whitehouse, M.J., Clocchiatti, R., 2012. Mantle source heterogeneity for South Tyrrhenian magmas revealed by Pb isotopes and halogen contents of olivine-hosted melt inclusions. Chem. Geol. 334, 266–279.

Roux, J., Lefevre, A., 1992. A fast quench device for HIPV. Eur. J. Mineral. 4, 279–281.

Salvioli-Mariani, E., Mattioli, M., Renzulli, A., Serri, G., 2002. Silicate melt inclusions in the cumulate minerals of gabbroic nodules from Stromboli volcano (Aeolian Islands, Italy): main components of the fluid phase and crystallization temperatures. Mineral. Mag. 66, 969–984.

Scaillet, B., Pichavant, M., Roux, J., 1995. Experimental crystallization of leucogranite magmas. J. Petrol. 36, 663–705.

Scaillet, B., Pichavant, M., Roux, J., Humbert, G., Lefèvre, A., 1992. Improvements of the Shaw membrane technique for measurement and control of fH_2 at high temperature and pressures. Am. Mineral. 77, 647–655.

Schiano, P., Eiler, J.M., Hutcheon, I.D., Stolper, E.M., 2000. Primitive CaO-rich, silica-undersaturated melts in island arcs: evidence for the involvement of clinopyroxene-rich lithologies in the petrogenesis of arc magmas. Geochem. Geophys. Geosyst. 1 (1999GC000032).

Schiano, P., Provost, A., Clocchiatti, R., Faure, F., 2006. Transcrystalline melt migration and Earth's mantle. Science 314, 970–974.

Schiavi, F., Kobayashi, K., Moriguti, T., Nakamura, E., Pompilio, M., Tiepolo, M., Vannucci, R., 2010. Degassing, crystallization and eruption dynamics at Stromboli: trace element and lithium isotopic evidence from 2003 ashes. Contrib. Mineral. Petrol. 159, 541–561.

Schmidt, M.W., Green, D.H., Hibberson, W.O., 2004. Ultra-calcic magmas generated from Ca-depleted mantle: an experimental study on the origin of ankaramites. J. Petrol. 45, 531–554.

Smith, I.E.M., Worthington, T.J., Price, R.A., Gamble, J.A., 1997. Primitive magmas in arc-type volcanic associations: examples from the southwest Pacific. Can. Mineral. 35, 257–273.

Sonzogni, Y., Provost, A., Schiano, P., 2010. Transcrystalline melt migration in clinopyroxene. Contrib. Mineral. Petrol. 161, 497–510.
Sorbadere, F., Schiano, P., Métrich, N., 2013. Constraints on the origin of nepheline-normative primitive magmas in island arcs inferred from olivine-hosted melt inclusion compositions. J. Petrol. 54, 215–233.
Takahashi, T., Hirahara, Y., Miyazaki, T., Senda, R., Chang, Q., Kimura, J.-I., Tatsumi, Y., 2013. Primary magmas at the volcanic front of the NE Japan arc: coeval eruption of crustal low-K tholeiitic and mantle-derived medium-K calc-alkaline basalts at Azuma volcano. J. Petrol. 54, 103–148.
Tatsumi, Y., Eggins, S., 1995. Subduction Zone Magmatism. Blackwell (211 p.).
Ventura, G., 2013. Kinematics of the Aeolian volcanism (southern Tyrrhenian Sea) from geophysical and geological data. In: Lucchi, F., Peccerillo, A., Keller, J., Tranne, C.A., Rosi, P.L. (Eds.), The Aeolian Islands Volcanoes. Geological Society, London, Memoirs Vol. 37, pp. 3–12.
Wood, B.J., Turner, S.P., 2009. Origin of primitive high-Mg andesite: constraints from natural examples and experiments. Earth Planet. Sci. Lett. 283, 59–66.
Zanon, V., Frezzotti, M.-L., Peccerillo, A., 2003. Magmatic feeding system and crustal magma accumulation beneath Vulcano Island (Italy): evidence from CO2 fluid inclusions in quartz xenoliths. J. Geophys. Res. 108 (B6). http://dx.doi.org/10.1029/2002JB002140.